Ocean Engineering 95 (2015) 34–58

Contents lists available at ScienceDirect

Ocean Engineering

journal homepage: www.elsevier.com/locate/oceaneng

Nature and magnitude of wave loadings at Seawave Slot-cone Generators

M. Buccino [a], D. Vicinanza [b,*], D. Salerno [c], D. Banfi [d], M. Calabrese [a]

[a] Department of Civil, Architectural and Environmental Engineering, University of Naples, Federico II Via Claudio 21, 80125 Napoli, Italy
[b] Department of Civil Engineering, Design, Building and Environment (DICDEA), Seconda Università di Napoli (SUN), Via Roma 29, 81031 Aversa (CE), Italy
[c] Maritime Engineering Division, Department of Civil Engineering, University of Salerno Via Giovanni Paolo II, 132-84084 Fisciano (SA), Italy
[d] School of Marine Science and Engineering, Plymouth University Drake Circus, Plymouth PL48AA, UK

ARTICLE INFO

Article history:
Received 13 May 2014
Accepted 30 November 2014
Available online 25 December 2014

Keywords:
Wave energy converters
Wave breaking
Wave loadings
Laboratory experiments
Scale effects

ABSTRACT

The Seawave Slot-cone Generator (SSG) is a wave energy converter based on the overtopping principle, which has collected a good deal of funds in the last years, from both public and private investors. Although its functional response has been extensively researched, practically no tools exist for the structural design. Based on the results of regular wave experiments conducted at the University of Naples *Federico II* (Italy), a number of design equations have been derived, which permit to estimate the magnitude of the wave pressures acting onto the outer face of the device, along with the respective rise times. The reliability of the predictive methods have been then verified against the random wave experiments of Vicinanza and Frigaard (2009).

1. Introduction

The high concentration of greenhouse gases in the atmosphere, about 400 ppm, makes the de-carbonization of the energy sector a binding need for the whole planet. For this reason clean energy investment is continuously increasing even in economically challenging times and has reached the amount of $ 244 billion in 2012 (REN21 Global Status Report, 2013).

The wave energy has the potential to be a particularly valuable contributor to a low-carbon energy mix, since, beside being very abundant (Brooke, 2003; Clement et al., 2002; Falnes, 2002), it has a different geographic distribution than wind and solar, greater predictability and less intermittency. Accordingly, even in the awareness that only a small fraction of this huge resource can be exploited, more than 1000 Wave Energy Converters (WECs) have been patented worldwide.

However, a number of prototype generators were destroyed in storms (Falcão, 2010), making evident that the lack of a specific knowledge on the capability of WECs of resisting wave actions may represent a serious hurdle, of both technical and economical nature, to the development of the devices.

Bearing this in mind, the Danish Council for Strategic Research has recently supported the project Structural Design of Wave Energy Devices (SDWED; Kofoed et al., 2010), whereas the European Commission has funded the GEOwave consortium (http://www.geowave-r4sme.eu), which brings together universities and private companies with the purpose of conducting industry specified research on anchoring and mooring systems expressly designed for WECs. Furthermore, in the development of an "integrated" overtopping-type WEC which uses a reservoir incorporated in a common rubble mound breakwater, Vicinanza et al. (2014) analyzed with much attention the nature of wave loadings acting on the tank, providing accurate methods for their prediction.

In this paper, the case of the Seawave Slot-cone Generator (SSG) is tackled. Patented by WavEnergy SAS (Stavanger, Norway), this device includes a number of reservoirs placed on the top of each-other, which capture the water during the up-rush phase (Fig. 1); on its way back to the sea, the fluid passes through a low head turbine, spinning it and producing electricity.

The WEC is normally located at the top of a steep foreshore, which has the purpose of increasing the potential run-up height; the latter will be nicknamed "*focuser*" in the following, as a reworked version of the term "*concentrator*" introduced by Polinder and Scuotto (2005) in describing the general functioning of the converters based on the overtopping principle.

The SSG technology has collected a good deal of funds in the last years and two pilot plants were planned to be located along

* Corresponding author.
E-mail addresses: buccino@unina.it (M. Buccino), diego.vicinanza@unina2.it (D. Vicinanza), dsalerno@unisa.it (D. Salerno), davide.banfi@plymouth.ac.uk (D. Banfi), calabres@unina.it (M. Calabrese).

http://dx.doi.org/10.1016/j.oceaneng.2014.11.038
0029-8018/

Nomenclature

Bgn	Bagnold number
C_{sample}	correction coefficient of pressures and forces considering the sampling effect
C_{scale}	correction coefficient of pressures and forces considering the scale effect
D	mean thickness of the air pocket
d	water level in the channel
E	expectation operator
$\hat{F}_{1/250}$	mean of the highest 1/250th peaks of force
F_{int}	integrated wave force
g	gravity acceleration
h	water depth at the toe of SSG
h_c	wall height
H	wave height
$H_{1/3}$	significant wave height
H_{m0}	significant (spectral) wave height
H/L	wave steepness
K_W	thickness of water mass effectively contributing to the impact
K_R	reflection coefficient
k	wave number
kd	relative water depth
L	wave length
L_{TP}	Linear Thrust Parameter
m	correction coefficient for $\hat{p}_{av}$
M_F	wave momentum flux through the base of the focuser
M_{FP}	Momentum Flux Parameter
p_0	atmospheric pressure
$\hat{p}$	pressure peak
$\hat{p}_{av}$	average pressure
$\hat{p}_{max}$	maximum pressure
r	correlation coefficient
R_c	crest freeboard of SSG
s_e	standard error
S	mean slope parameter
S_0	still water thrust at the base of the focuser
t_r	peak rise time
$tg\alpha_{av}$	average value of the slope
T	wave period
$T_{1/3}$	significant wave period
T_p	peak wave period
u	cross-shore wave velocity
u_0	velocity of the water hammer
X	vector of the log-variables
z	vertical coordinate
Z_G	vertical distance of pressure barycentre from the structure toe
η	free surface
λ_F	Froude scale factor
λ_S	scale correction factor
μ	vector of averages of the log-variables
Π_x	horizontal component of the peak force exerted on the structure
ξ	inshore Iribarren number
ρ	water density
Σ	matrix of covariance

the West Norwegian coasts; one at the isle of Kvitsøy (in the Bokna fjord), the other around Svåheia (Fig. 2).

The extensive investigations carried out on the hydraulic performances of the device (Margheritini et al. 2009; Vicinanza et al., 2012), allowed deriving a number of equations where the amount of water entering the reservoirs can be reliably estimated under different wave conditions, including oblique and short-crested seas. Conversely, practically no tools exist for the structural design.

In this respect, the wider experimental study available to date is that of Vicinanza and Frigaard (2009), which though could not lead to any general conclusion, since the tests reproduced the specific climate of the site of Kvitsøy. Successive investigations conducted during the design of the Svåheia plant (e.g. Buccino et al., 2011) encompassed a very narrow set of data, with a limited variance of the hydraulic parameters.

Therefore, to fill the gap new experiments have been performed at the University of Naples *Federico II* (Italy). Here, the wave parameters have been varied enough to get a wide spectrum of loading cases. Moreover, it has been chosen to work with regular waves to study the structure response under very simple forcings. From the analysis of data a set of design tools have been derived, the reliability of which have been then checked against the random wave experiments of Vicinanza and Frigaard (2009).

The article is organized as follows. After a description of the experimental set-up (Section 2), the Sections 3 and 4 discuss the qualitative features of the observed wave profiles and of the actions they induce on the SSG. In Section 5, a preliminary map for the prediction of the different loading cases is presented. A probabilistic design tool for the estimation of the peak pressures acting on the front face of the wall is given in Section 6. The predictive method is finally compared to random wave data in Section 7.

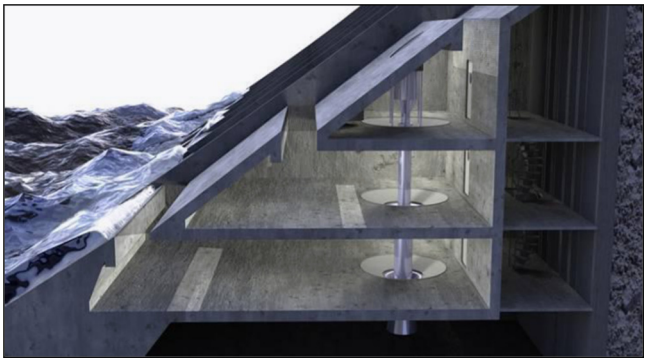

Fig. 1. Artistic representation of a 3-level SSG.

2. Experimental work

2.1. Facility and model

The experiments have been carried out at the *Small Scale Channel* (SSC) of the *Laboratorio di Ingegneria Costiera* (*LInC*) of the Department of Civil, Architectural and Environmental Engineering (*DICEA*) of the University of Naples *Federico II*. The flume, 22 m long, 0.5 m wide and 0.75 m deep, is equipped with a piston-type wavemaker capable of generating both periodic and random wave series. The facility is also provided with an active absorption system, to dampen any undesired reflection generated by the structures installed within it.

The *SSG* was a 1:66 scale model of the Svåheia pilot plant (Fig. 3); it was made of plexiglass, with the front plates inclined by 35° to the horizontal.

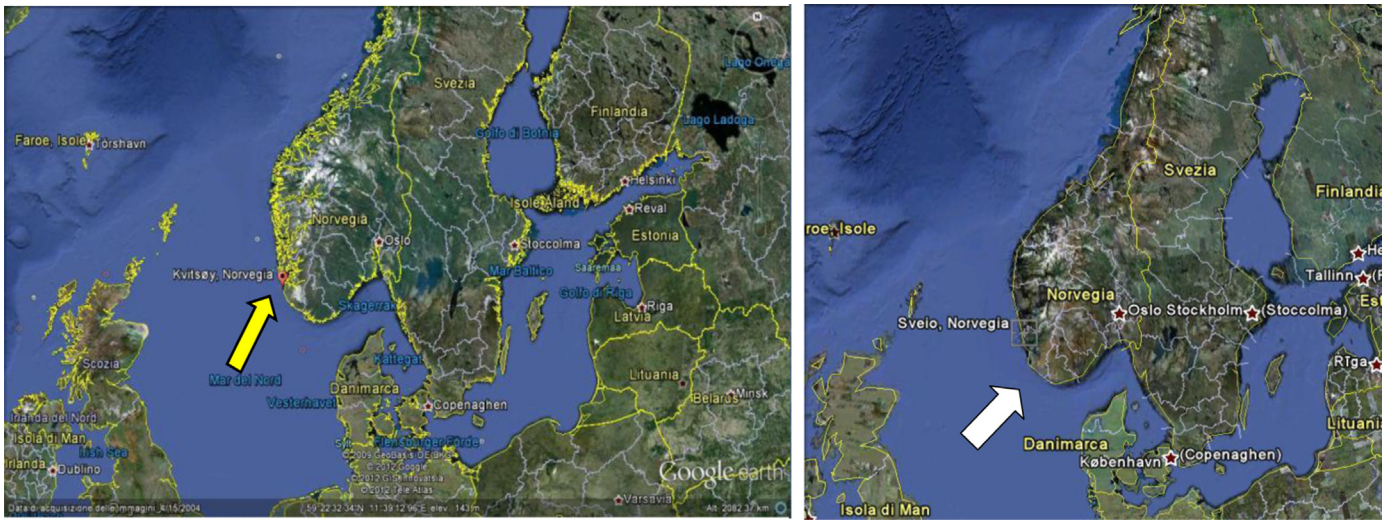

Fig. 2. The sites of Kvitsøy (left panel) and Sväheia (right panel).

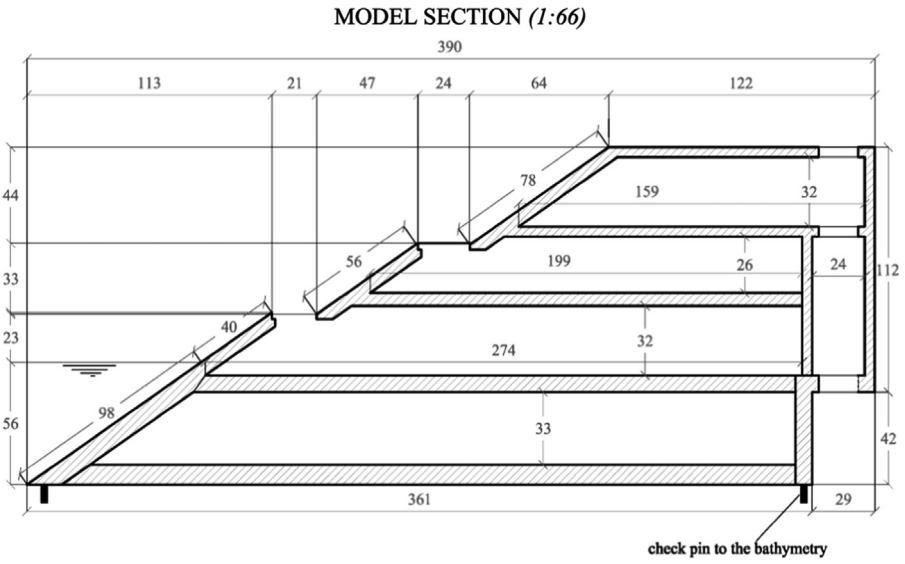

Fig. 3. Sketch of the SSG model. Dimensions in mm.

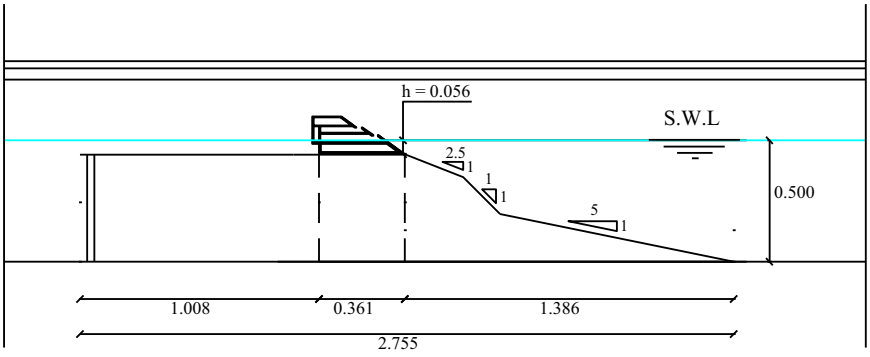

Fig. 4. The bathymetry and the location of the WEC. Dimensions in m (model scale).

Along with the *WEC*, also the steeper part of the foreshore (the "*focuser*") has been reproduced at the same scale (Fig. 4). The beach extended about 1.39 m towards the wavemaker and included a 1:5 approaching slope followed by two ramps with an inclination of respectively 1:1 and 1:2.5. Between the toe of the approaching slope and the wavemaker, the bottom of the flume was flat.

The *SSG* has been seated on a horizontal strip of plexiglass extending about 1 m beyond its heel.

All tests were conducted with a water level in the channel, $d=0.50$ m; accordingly, the WEC had the crest freeboard (R_c) 0.10 m above the swl, whereas the water depth at its toe, h, was 0.056 m.

2.2. Waves

Thirty-one regular wave trains with a duration of 128 s have been run, divided into four subsets of constant period, *T*. The values of the latter (0.8 s, 1.0 s, 1.5 s, 2.0 s) were chosen in order to get a range of relative water depths, *kd*, spanning from deep waters ($> \pi$) to quasi-shallow waters (< 1).

The incident wave heights at the toe of the "*focuser*" were varied between 2.6 cm and 22 cm; this gave values of the wave steepness ranging from 0.006 to 0.124. No waves have been observed to break seawards the approaching slope.

2.3. Control of water level behind the device

During the tests, the water passing over the roof of the *SSG* was conveyed back to the wave-maker via a submersible pump with a maximum capacity of 375 l/min (Fig. 5). The pump was lodged in a 0.147 m^3 reservoir built about 4 m off the trailing edge of the structure. A valve permitted to control the amount of discharge.

A porous mound, made of cobblestone, has been placed between the model and the reservoir to absorb the waves generated by overtopping in the sheltered area.

2.4. Measurements

Four twin-wire resistive probes sampled at 25 Hz were placed seaward the "*focuser*" to separate incident and reflected waves through the method of Zelt and Skjelbreia (1992), which is based on a weighted least square approach. The separation procedure has been applied to the band 0.5–1.5 the fundamental wave frequency. For the analysis to be as reliable as possible, the probes position has been optimized test by test using the frequency response function suggested by *Zelt and Skjelbreia* at the Eq. (20) of their paper.

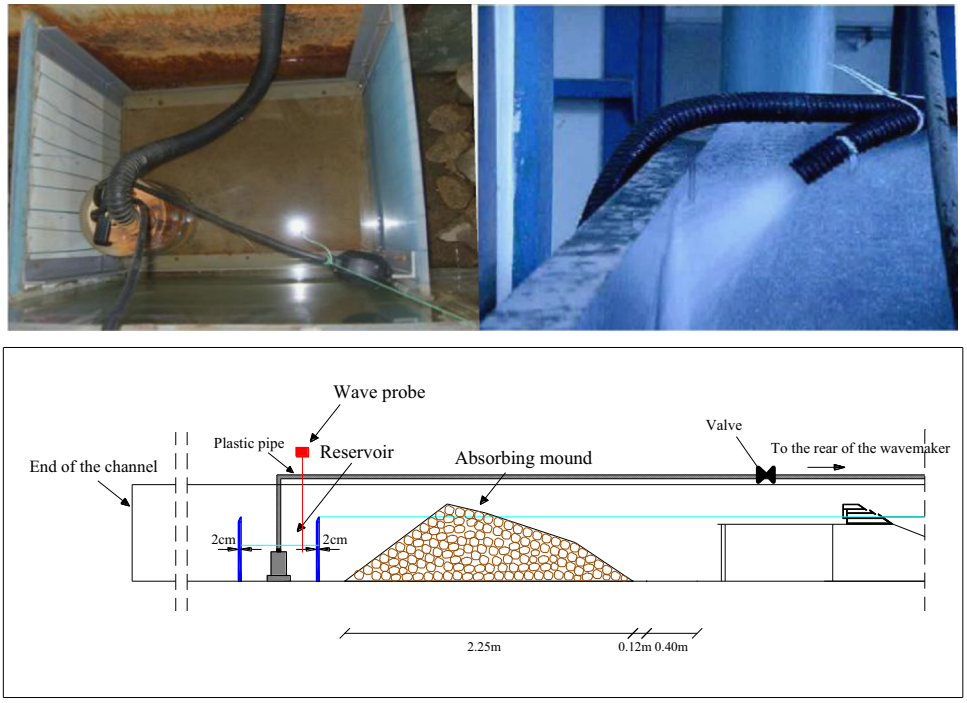

Fig. 5. View of the recirculation system. Top panels: reservoir (left) with pump and plastic pipe at the rear of the wavemaker (right). Low panel: general sketch of the system.

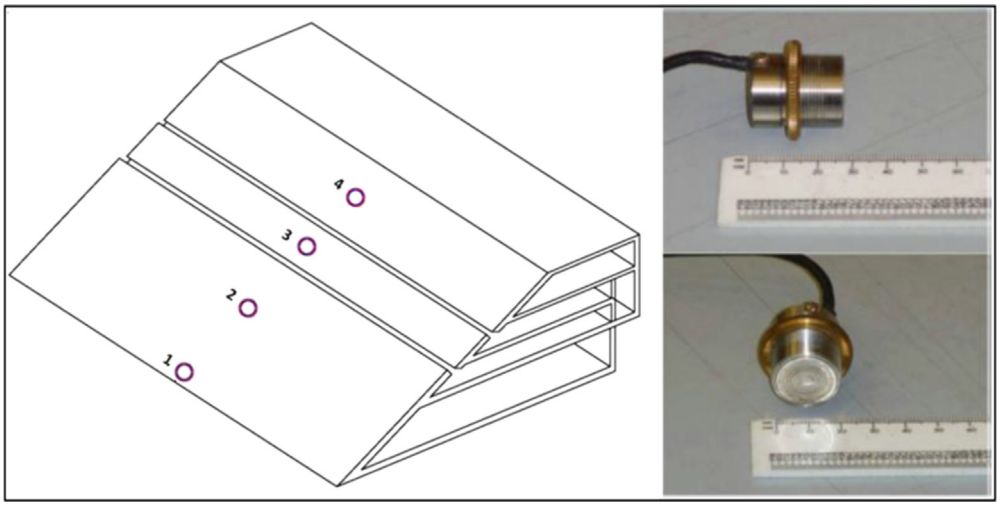

Fig. 6. Position and features of the pressure transducers.

As shown in the low panel of Fig. 5, an additional wave gauge was used to check the water level in the reservoir during the pumping process.

Four piezo-resistive pressure transducers with a cut-off frequency of 20 kHz were positioned along the outer plates of the *SSG*, according to the scheme of Fig. 6 (see also Table 2). The sensors had a diameter of 18 mm and were sampled at 1 kHz.

The center of the transducer "p_1" was 1.40 cm above the toe of the wall, whilst "p_2" recorded the pressure signal at the swl. "p_3" and "p_4" were located in the middle of the second and third plate respectively, where Vicinanza and Frigaard (2009) measured the maximum values of loadings. The center of the transducer "p_4" was 2.35 cm below the top of the *WEC*.

A digital video camera was employed to record the macroscopic features of the wave profiles.

2.5. Data processing

From the application of the *Zelt and Skjelbreia* method, the time-domain fluctuations of the incident and the reflected wave profiles were obtained. As mentioned before, these signals were limited in the band 0.5–1.5 the fundamental frequency of the waves. The chronograms were subjected to zero up crossing and for each of them the wave height and period have been conventionally assimilated to the mean of the highest third of the waves ($H_{1/3}$ and $T_{1/3}$). This is consistent with the suggestions of Goda (1986).

Dividing the reflected wave height by the incident one, the reflection coefficient K_R has been obtained, which obviously refers to the whole model including the foreshore and the *SSG*.

As far as the pressure data is concerned, the following quantities have been calculated for each wave period and each transducer:

- the pressure peak $\hat{p}$, i.e. the maximum pressure over a wave cycle;
- the peak rise time t_r, i.e. the time interval between the pressure levels corresponding to the 2.5% and the 97.5% of the peak value $\hat{p}$. Note that for a simple sine wave, t_r equals approximately 0.21 T.

These data series (peaks and rise times) have been treated as samples of random variables and the respective cumulative distribution functions (*cdf*) have been estimated.

The pressure signals have been then spatially integrated, using the trapezium rule, to get an estimate of the wave force time history F_{int} (t). To this purpose, the pressure chronograms at the edges of the *WEC* (top and toe) have been reconstructed extrapolating linearly the signals of the two closest transducers (p_1 and p_2 for the toe and p_3 and p_4 for the top).

Like for the pressures, also for F_{int} (t) the *cdf*s of peaks and rise times have been estimated.

Finally the chronogram of the application point of the wave force has been obtained, calculating the pressures barycentre instant by instant, including the fictional values at the ends of the wall.

3. Observed wave profiles

It has long been recognized in literature (Peregrine, 2003; Oumeraci et al., 1994) that the shape of the wave as it meets the structure has a strong influence on the nature and magnitude of the resulting loadings. Although the wave profiles observed in the present experiments do not differ a great deal from those reported in the classic studies on sloping beaches, a brief discussion is however provided to render the terminology employed in the next paragraphs as clear as possible.

For the smallest wave heights producing no overtopping, *quasi-standing* wave patterns were observed, in which the free surface at the wall oscillated between a convex profile, corresponding to the run-down phase, and a concave shape, corresponding to run-up (Fig. 7). The inherent inefficiency of the reflected wave generation via down-rush (Cross and Sollitt, 1972), aggravated by the segmented contour of the structure face, reduced the values of the reflection coefficient within the range 0.61–0.79, that is well below the unity.

With the occurrence of breaking, the free surface was seen to become nearly vertical in some part of the wave front and a jet of fluid, referred to as *plunging jet* in the following, protruded forwards. Just depending on the position of the *plunging jet* at the incipient breaking, three wave shapes have been distinguished, namely *surging*, *collapsing and plunging* breakers.

In the case of *surging breakers*, the jet detaches from the toe of the wave when the water motion reverses from down-rushing to up-rushing. (Fig. 8a). The water tongue falls over a small cushion of water preceding the vertical part of the front, producing a very turbulent zone where most of the energy is lost (Fig. 8b). Yet, this "dissipation area" does not propagate forward and when the crest of the wall is reached and overtaken, the air bubbles are significantly re-absorbed into the fluid (Fig. 8c). Values of K_R between 0.38 and 0.68 have been measured, due to the effects of both the wave energy dissipation and overtopping.

Owing to the size of the turbulent toe, the above description of *surging breaker* is rather similar to that given by Iversen (1952); on contrary, it differs from the definition suggested by Galvin (1968) who used the term "*surging*" to indicate a limiting case in which the "dissipation area" diminished to zero.

For the *collapsing breakers*, the rupture takes place well beyond the phase of run-down; the plunging jet is located significantly above the toe of the wave, but still below the crest (Fig. 9a). This description is essentially the same as those given by Galvin (1968) and Basco (1985). Compared to the case of surging breakers, the plunging jet has a larger momentum and hits violently the sea

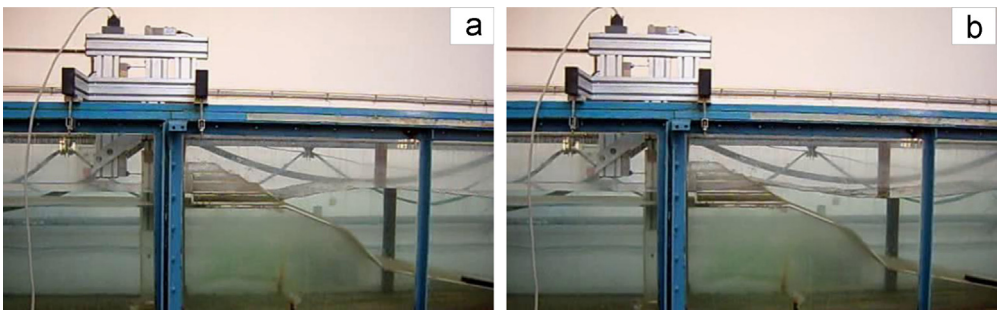

Fig. 7. Example of quasi standing wave (H=0.036 m, T=1 s): (a) wave shape at run-down and (b) wave shape at run-up.

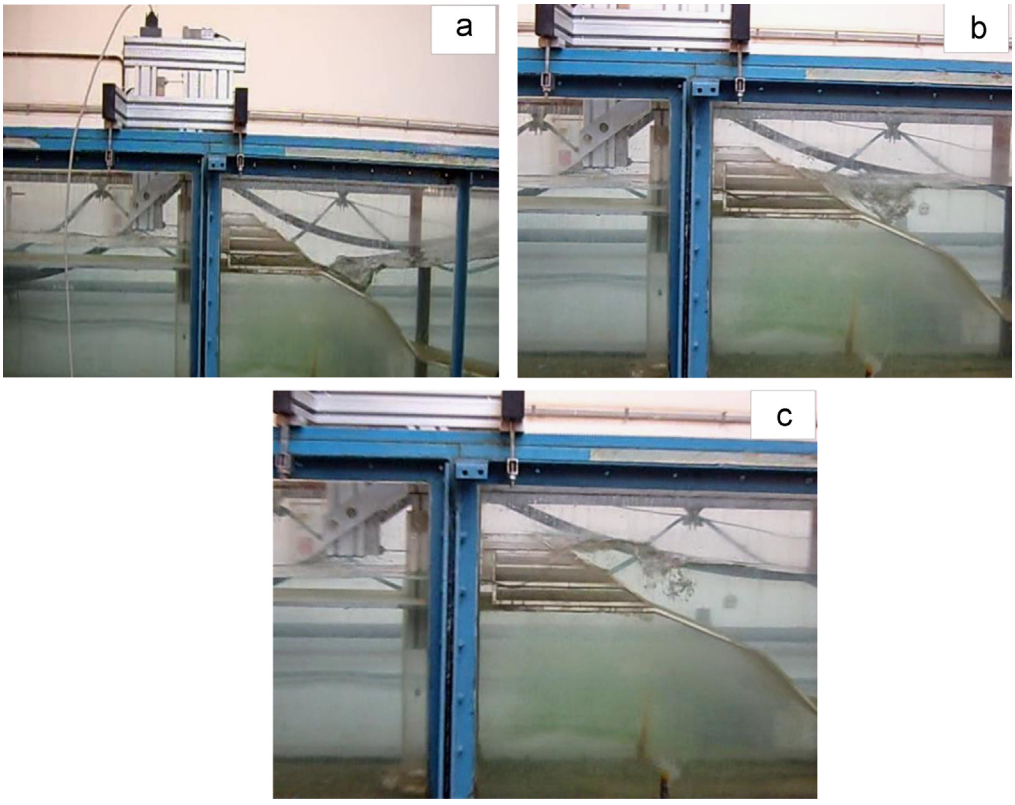

Fig. 8. *Example of Surging breaker* (H=0.076 m, T=2 s).

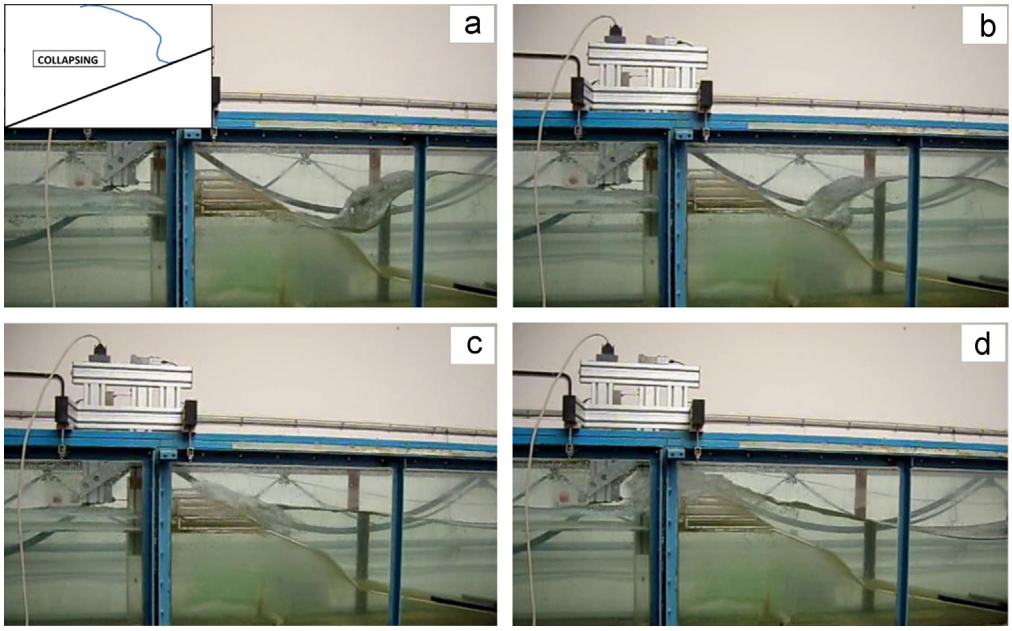

Fig. 9. Example of Collapsing breaker (H=0.15 m, T=1.5 s). The sketch reported in the upper left corner of panel "a" has been re-drawn from Galvin (1969).

bottom (Fig. 9b) prior to splash up against the WEC (Fig. 9c) and overtop the roof (Fig. 9d). Due to the intense dissipation of energy and the large wave heights (Table 1), the reflection coefficient has been found to be included between 0.10 and 0.56.

In the case of *plunging breakers*, the jet moves from the crest (Fig. 10a); the wave profile behind the breaking area is then horizontal or descending, whereas it was rising for *surgings* and *collapsings*. In the present experiments the breaking initiated close enough to the *SSG*, to allow the plunging jet slamming the structure about its toe (Fig. 10b). After the "hammer shock", an

Table 1
Summary of main hydraulic parameters. H refers to the measured values of the incident wave heights.

# tests	T[s]	d [m]	L [m]	H [cm]	kd	H/L	H/d	R_c/H
8	*0.80*	*0.50*	*0.99*	*4.92–12.25*	*3.17*	*0.050–0.124*	*0.10–0.24*	*0.82–2.03*
8	*1.00*	*0.50*	*1.51*	*3.59–15.42*	*2.08*	*0.024–0.102*	*0.07–0.31*	*0.65–2.78*
8	*1.50*	*0.50*	*2.78*	*3.56–21.92*	*1.13*	*0.013–0.079*	*0.07–0.44*	*0.46–2.80*
7	*2.00*	*0.50*	*4.02*	*2.58–16.21*	*0.78*	*0.006–0.040*	*0.05–0.32*	*0.61–3.87*

intense splash-up is produced (Fig. 10c). The measured reflection coefficients ranged from 0.15 to 0.58.

Both in case of *plunging* and *collapsing* breakers, an air pocket is trapped beneath the plunging jet, which is then compressed and destroyed by the incoming water mass.

4. Wave loadings macro-characteristics

4.1. General description

The actions produced by quasi-standing waves are of *pulsating* (or *quasi-static*) type; this kind of loadings are dominated by the effect of gravity and the rise times are of the same order as the period of waves. Likely due to the low values of the wave steepness tested (not larger than 0.04), the time-histories of the wave force at the wall have been observed to possess the same shape as the waves at the toe of the "*focuser*". An example is given in Fig. 11a, where the chronograms of the wave profile and F_{int} have been standardized and limited to their positive part, to ease the comparison. Together with forces also the pressures at the swl have the same pulsating character (Fig. 11b).

The spatial distribution of pressures *at the peak of force* resulted approximately bi-trapezoidal, with the maximum at the swl (Fig. 11c); the vertical distance of the pressures barycentre from the structure toe, Z_G, has been found to not exceed 0.35 times the wall height, h_c (Fig. 11d).

Table 2
Details of pressure sensors positions.

Code	Transducer centre to the SSG toe (cm)	Description
p_1	*0.014*	*Toe of the SSG*
p_2	*0.056*	*SWL*
p_3	*0.094*	*Middle of 2nd plate*
p_4	*0.132*	*Middle of 3rd plate*

However trivial it may seem, another remarkable feature of this loading case is its repeatability under a regular wave attack; in the example shown in Fig. 11e, more than 90% of the peaks of F_{int} are included in the interval 3.9–4.1 kg/m, whereas the corresponding rise-times lie in the range 0.2 *T*–0.23 *T* (Fig. 11f).

For *surging and collapsing breakers with small wave heights*, the loading process remains quasi-static and repeatable, with a pressure distribution at the peak of force still bi-trapezoidal (Fig. 12 left panel). Yet, due to the wave overtopping, the centre of mass of such distribution is located almost invariably at half the structure height (Fig. 12 right panel). This is the same as supposing the pressure to be constant along the *SSG*, in accordance to the hypothesis formulated by Hiroi in the early '900 for vertical breakwaters.

This analogy is most likely explained by the fact that in the Japanese design practice, vertical breakwaters are allowed to be significantly overtopped during the design storms (Goda, 1995).

With increasing the wave height, the big mass of water involved in the process of up-rush attains such velocities and accelerations to generate moderate impact events ($\hat{p}$ still of the order of *H*).

A deeper insight on the video camera recordings revealed that as the steepness grows, the wave crest tends to reach quickly the "breaking area" at the toe of the front, collapsing on it and then hitting the wall (Fig. 13). The presence of foam and air bubbles dampens the intensity of the impact.

This phenomenon, which is still relatively slow, causes the appearance of a higher and sharper peak of force before the pulsating smooth one (Fig. 14a). The ratio between the two maxima may reach and overcome 2. At the same instant when wave force reaches the peak, the maximum pressure is not recorded at the swl, but above it (Fig. 14b). Depending on the amount of water involved, the "impact" may be either localized above the swl (with the lower pressures remaining pulsating) or extend throughout the structure height, like in the case of the low panels of Fig. 14.

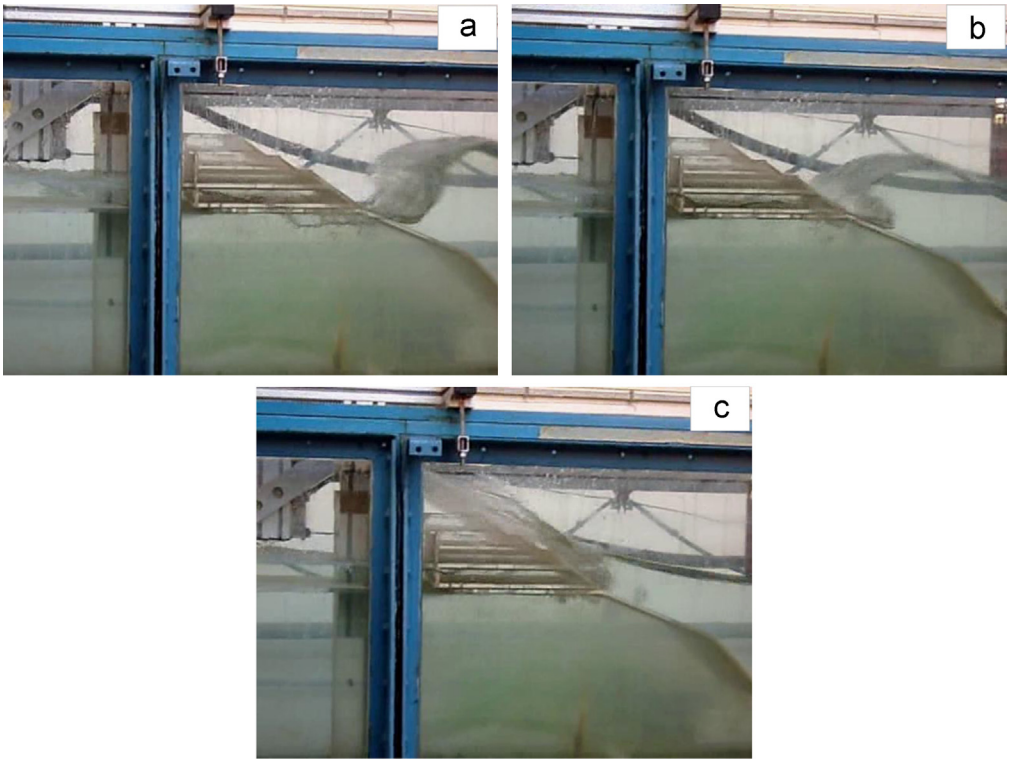

Fig. 10. *Example of Plunging breaker* ($H=0.11$ m, $T=1.0$ s).

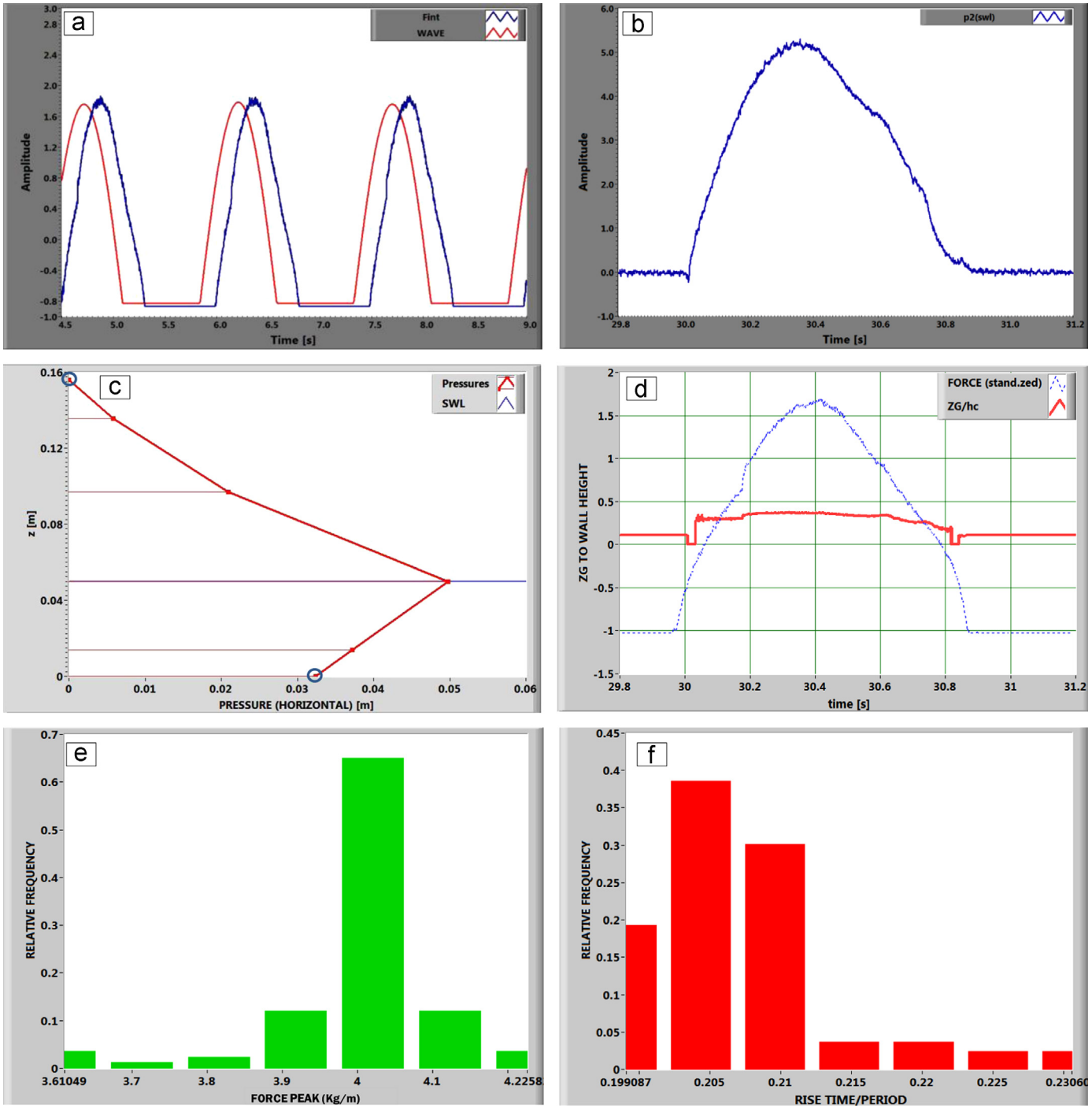

Fig. 11. Characteristics of loadings generated by quasi-standing waves (H=0.036 m, T=1.5 s). (a) time-histories of F_{int} and wave profile at the toe of the focuser; (b) time-history of the wave pressure at the swl (in cm); (c) spatial distribution of loadings at the force peak (blue circles indicate extrapolated data); (d) time-history of the pressure barycentre; (e) and (f) histograms of the peaks of force (in kg/m) and of the corresponding rise-time to wave period ratio.

Under these conditions a real steady state seems to be not reached, and accordingly repeatability is lost; under the same periodic attack, small impacts may alternate to pulsating patterns.

It is noteworthy that the lack of repeatability applies also to the spatial distribution of pressures, which may have the maximum either at swl (pulsating events) or at different positions above it (Fig. 15a-c-e).

Yet, in spite of this variability, Z_G seems to undergo, at the peak of force, only slight fluctuations around the value 0.5 h_c (Fig. 15b-d-f). This result is rather interesting because, as partially mentioned before, would allow substituting the actual distribution of loadings, highly variable, with its average value, that is expected to be more stable and predictable. Nevertheless, given the low number of pressure transducers here available, an accurate validation against new data sets is desirable. A first check is carried out in the Section 7 of this article.

Under *plunging breakers*, the slamming of the plunging jet onto the structure (hammer shock) generates a severe impulsive force peak, as shown in Fig. 16a. When the maximum of F_{int} is reached, the pressure magnitude at and above the swl is generally zero and the spatial distribution of loadings might be assumed triangular, with the maximum around the toe of the structure (Fig. 16b). The impact event has a rise time extremely short (t_r O(0.001 T)) and is

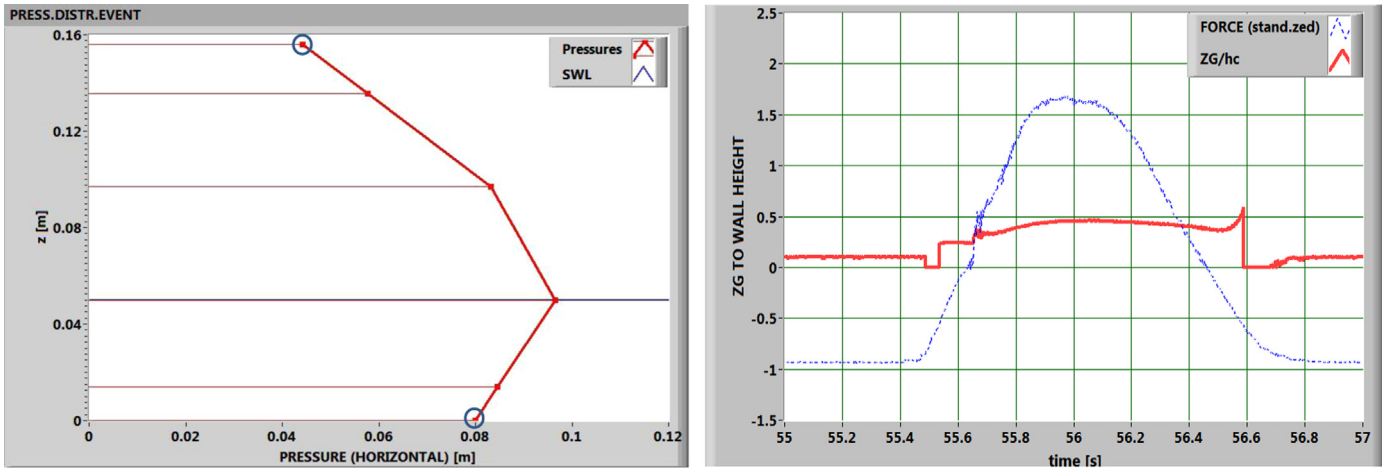

Fig. 12. Characteristics of loadings for a small collapsing breaker ($H=0.07$ m, $T=1.5$ s). Left panel: spatial distribution of pressures at the force peak (circles indicate extrapolate values). Right panel: time-history of the pressures barycentre.

Fig. 13. Surging breaker with large wave height ($H=0.16$ m, $T=2$ s). Left panel: the crest of the wave reaches the dissipation area at the toe of the front. Right panel: the water tongue hits the SSG and overtops the roof.

followed by a number of oscillations due to the compression of the air trapped during the crest overturning (see Fig. 10b).

Examining the pressure signals in the low panels of Fig. 16, it is noted that the peaks of p_2 and p_3 are about one order of magnitude lower than p_1; this underlines the essentially local nature of the loading case. Moreover, a sort of "secondary strike", much less intense than the main one, occurs at the transducer p_4 because of the splash-up subsequent to the crest falling.

Since the impact mechanism is significantly affected by the amount of air entertained in the water, and even by small disturbances of the free surface (Peregrine, 2003), the resulting loadings exhibit a large variance. A typical example is displayed in the histograms of Fig. 17, which refer to the transducer p_1 and the same experiment as in Fig. 16. The pressure peaks (relative to H) and the corresponding rise time to wave period ratios span over an entire order of magnitude; interestingly, the modal value of the former is located between 1 and 2, suggesting that violent impacts (peaks as large as 10 H) are in fact "tail events" with low exceedance probability.

More generally, the impulsive pressure peaks measured in the present experiments are significantly lower than those reported in literature for vertical and sloping face breakwaters. For example, the 10% exceedance probability value of $\hat{p}/\gamma H$has been found to not exceed 5, whereas Kirkgoz (1995) measured 14.5 on walls inclined by 45°.

This big difference is mainly due to the macro-features of the breaking process. While in the Kirkgoz experiments the waves arrived almost flat at the structure, and the breaking initiated very close to the wall with nearly no trapped air (the author referred to this situation as *perfect breaking*), the impacts observed in the present tests occurred well after the wave had begun to break, so that a significant amount of air could be hold beneath the crest (Fig. 18).

This breaking morphology, which tends to reduce the risk of violent impacts, is favored by two characteristics that are peculiar of the *SSG* design, namely the shallow foreshore in front of the structure and the relatively mild inclination of the outer plates; the former causes the waves to attain the incipient breaking condition prior reaching the wall, whereas the latter obliges the breaker to perform a nearly 55° rotation to hit the structure.

4.2. Classification of wave forces

The patterns of *wave force* (F_{int}) previously described have been grouped into three classes, based on the definitions introduced for vertical breakwaters by the PROVERBS project (Oumeraci et al., 1999; Allsop and Vicinanza, 1996; Allsop et al., 1996). Thus, a force chronogram is termed *pulsating* if it exhibits a unique smooth peak over a wave period. A double peak pattern is instead named either *slightly breaking* or *impact*, depending on whether the first sharp maximum is lower or larger than 2.5 times the second peak.

It is worth to point out that, owing to the inherent variability of the force chronograms under breaking waves, the classification above has been conventionally referred to the modal (most frequent) features observed in each test.

5. Preliminary parametric analysis on breaker types and loading cases occurrence

For maritime structures subjected to loadings of highly variable nature, it is central to have a design tool which allows predicting

the occurrence of one or another of the force types. For vertical breakwaters, examples of such kind of implement are the graphs of Nagai (1973) and Nagai-Otsubo (1974), the decision tree of Goda (1986), the Parameter Map (Oumeraci et al., 1999) and the Calabrese's criterion (Calabrese and Buccino, 2000).

Unfortunately, the present set of data is not wide enough to lead to a robust method for the specific case of *SSGs*; yet, a parametric analysis is conducted below, with the twofold aim of introducing the main governing variables and achieving a preliminary scheme to be used as starting point for future research works.

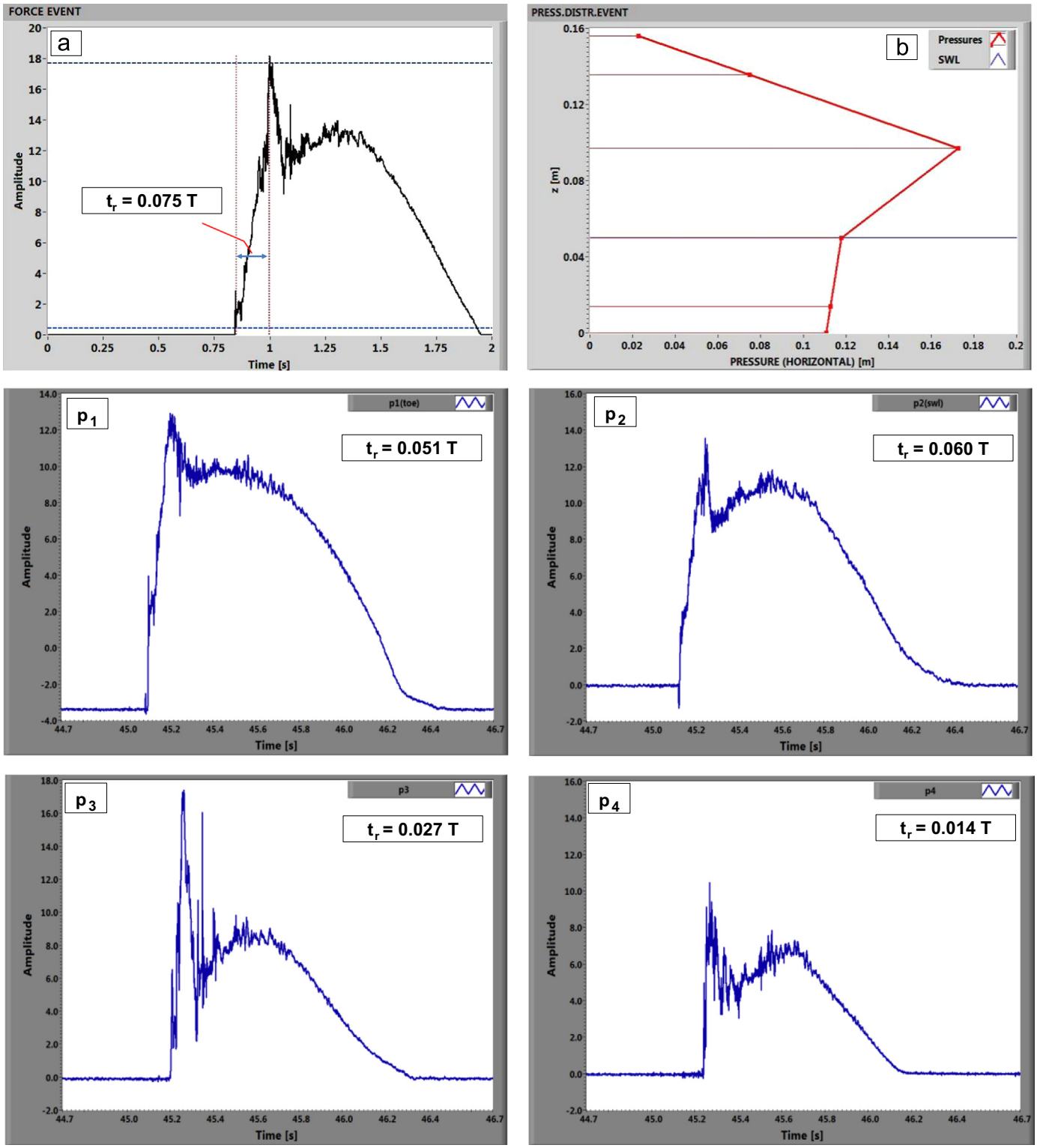

Fig. 14. Characteristics of loadings generated by a surging breaker with large wave height (H=0.16 m, T=2 s). (a) horizontal force time-history (kg/m); (b) spatial distribution of pressures at the peak of force. Low panels: time-histories of the wave pressures (in cm).

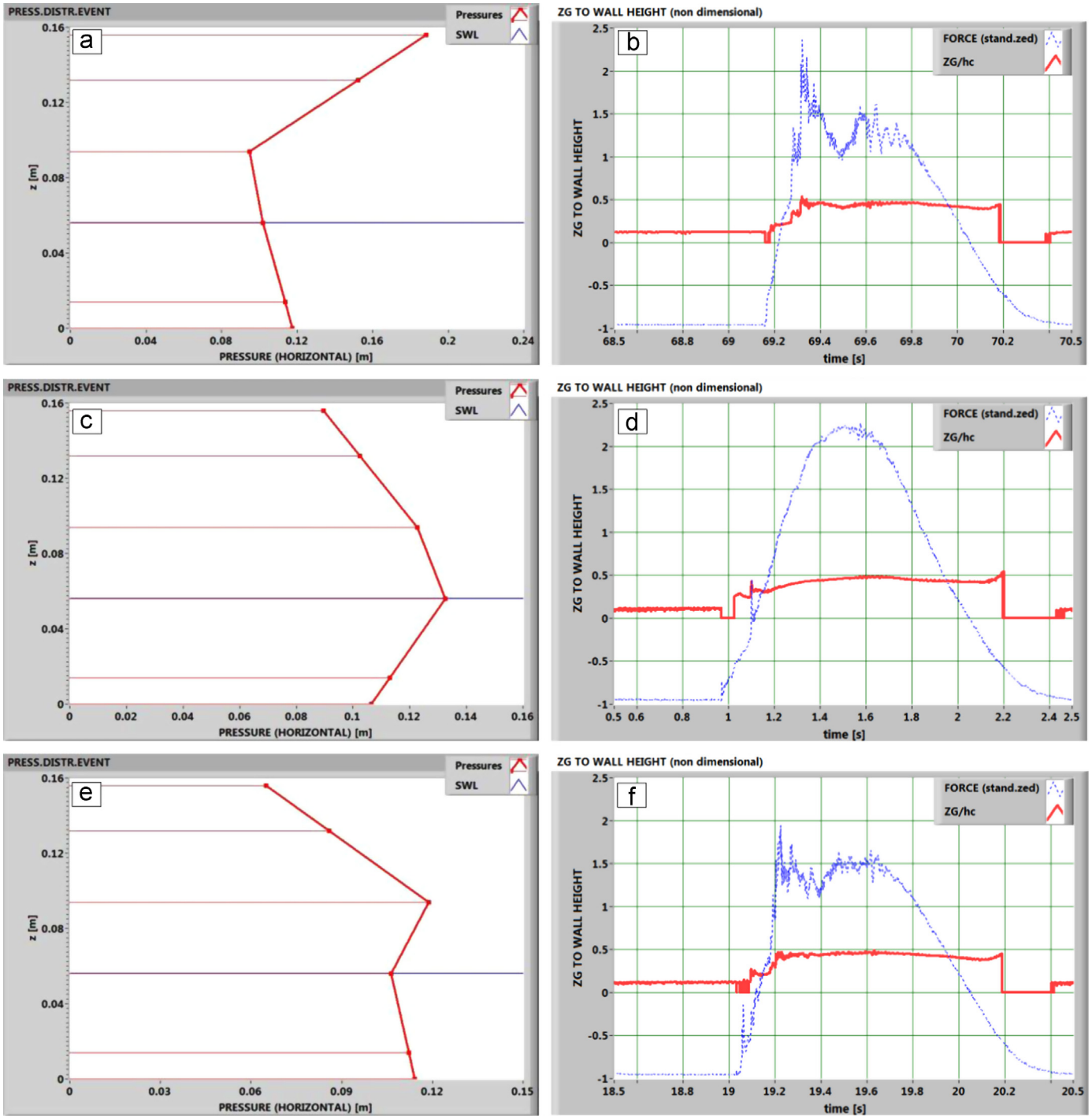

Fig. 15. Force events for a surging breaker with large wave height (H=0.16 m, T=2 s).

The non-dimensional quantities employed are essentially three. One is the well-known *surf similarity parameter* or *inshore Iribarren number* (Battjes, 1974):

$$\xi = \frac{tg\alpha_{av.}}{\sqrt{2\pi H/gT^2}} \quad (1)$$

in which H is the *incident* wave height at the toe of the *focuser*. As for the slope at the numerator, the average value from the toe of the bathymetry to the top of the *SSG* has been taken ($tg\alpha_{av.}$, Fig. 19), to render the comparison with other data sets as simple as possible. Compared to the average slope angle suggested by Zanuttigh and Van der Meer (2008), who proposed to take the mean between the points at $\pm$ 1.5 H around the swl, $tg\alpha av$ also accounts the inclination of the foreshore prior the breaking point, which is important to distinguish among the various breaker types. Furthermore, it allows maintaining bottom and wave parameters separated in the Iribarren number of Eq. (1), thus simplifying the interpretation of the results.

The second quantity is the (mean) "*slope parameter*" (Svendsen, 2006), which is widely used in literature for both wave propagation and wave reflection problems. It basically represents the ratio

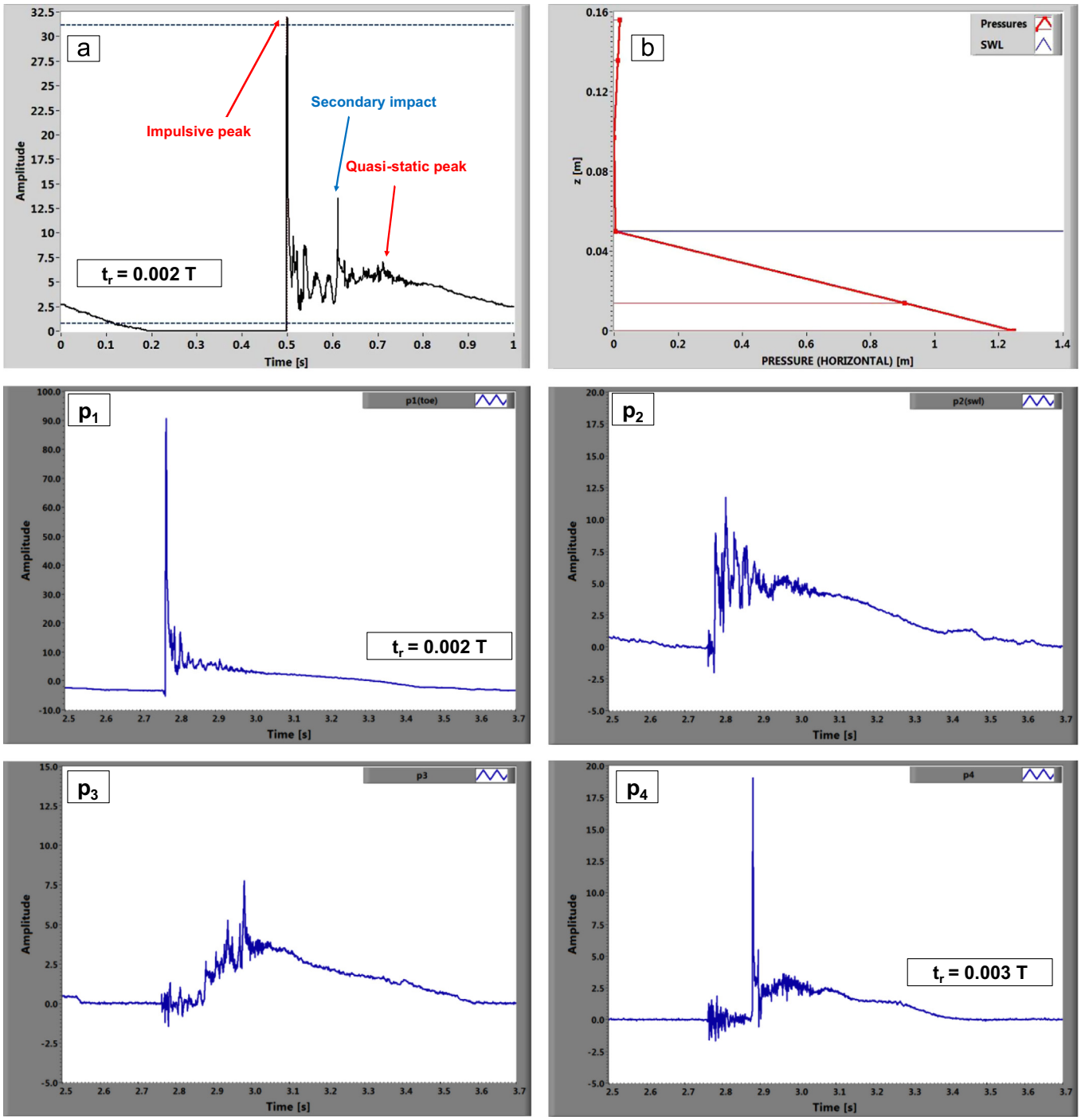

Fig. 16. Characteristics of loadings generated by a plunging breaker (H=0.11 m, T=1 s). (a) horizontal force time-history (kg/m); (b) spatial distribution of pressures at the peak of force. Low panels: time-histories of the wave pressures (in cm).

between the length of the waves and the mean horizontal distance between the toe of the foreshore and the shoreline:

$$S = \frac{tg\alpha_{av.}}{kd} \tag{2}$$

In the Eq. (2), the wavenumber k has to be evaluated on the flat bottom, where the still water depth equals d.

The third variable will be referred to as *Linear Thrust Parameter* (L_{TP}) hereafter and is a linearized- slightly-modified form of the *wave Momentum Flux Parameter* (M_{FP}) originally introduced by Hughes (2004).

We consider the ratio between the maximum value (over a wave period) of the cross-shore component of the wave momentum flux through the base of the *focuser* (M_F) and the corresponding hydrostatic still water thrust (S_0):

$$\frac{M_F}{S_0} = [max]_{t\ \epsilon\ T} \frac{\int_{-d}^{\eta} (p+\rho g z+\rho u^2)\, dz}{\left(\frac{1}{2}\rho g d^2\right)} \tag{3}$$

where η is the free surface, z is the vertical coordinate (positive upwards), u is the cross-shore wave velocity, ρ is the water density and g is the gravity acceleration.

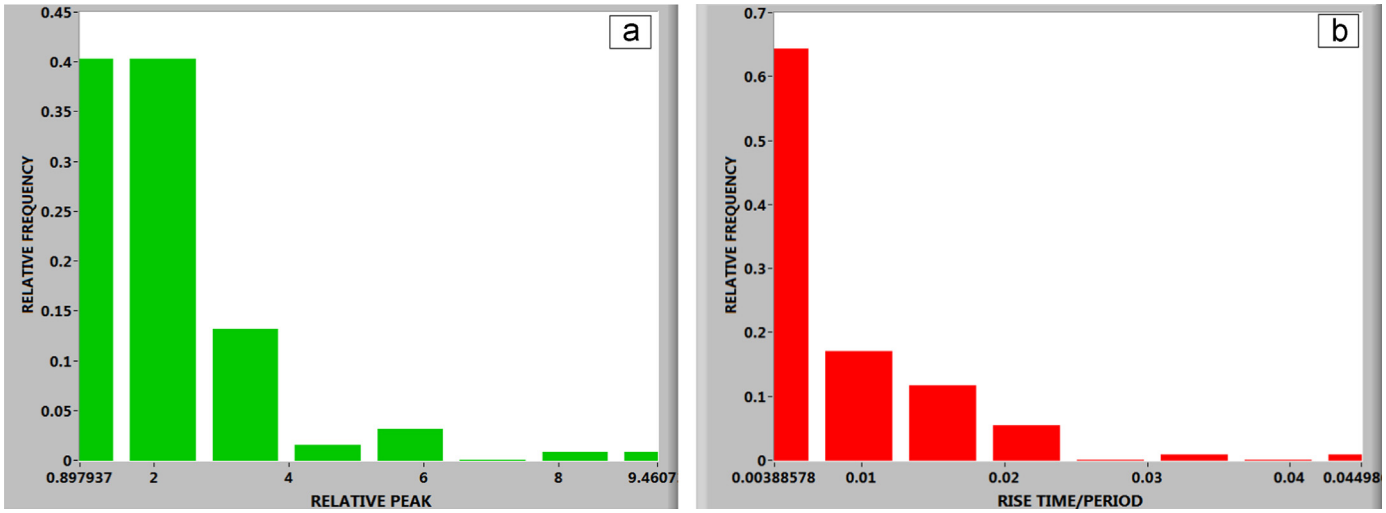

Fig. 17. (a) Histogram of the peaks of pressure, relative to the incident wave height, for the transducer p_1 (H=0.11 m, T=1 s). (b) histogram of the corresponding rise-time to wave period ratio.

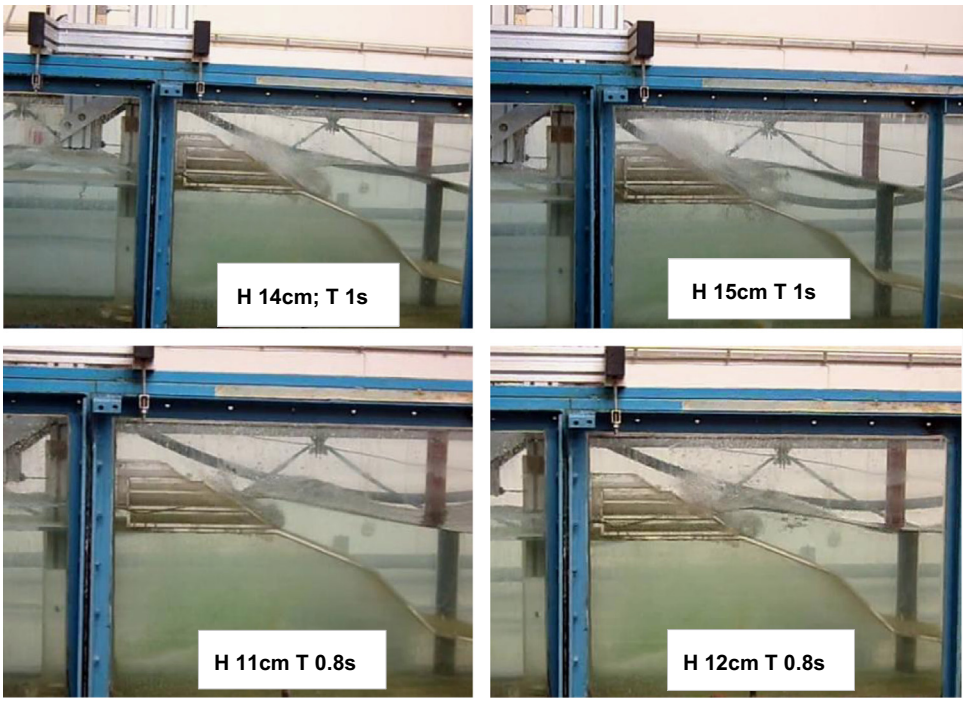

Fig. 18. Examples of plunging breakers profiles at the structure.

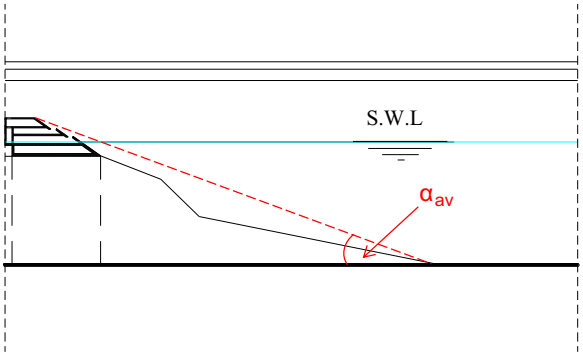

Fig. 19. Definition of the mean slope angle.

Eq. (3) coincides with the definition of M_{FP}, apart from the introduction of the coefficient ½ at the denominator. By using the linear wave theory and retaining only the first order terms, one gets:

$$L_{TP} = \frac{H}{d}\frac{tanh(kd)}{kd} \tag{4}$$

which in fact represents the excess of pressure thrust at the toe of the slope due to the presence of waves. It is useful to remark that the main difference between M_{FP} and L_{TP} is that the former is inherently non-linear in H (Hughes 2004), whereas the latter is by definition. It is finally noticed that in shallow waters L_{TP} tends to the wave height to depth ratio H/d.

It is important to emphasize that only two of the above governing quantities are independent, since it can be shown that:

$$\sqrt{\frac{L_{TP}}{2\pi}}\xi = S \tag{5}$$

In Fig. 20, L_{TP} is on the ordinates and the Iribarren number is on the abscissas; on this plane, all the variables relevant to the breaking process (slope angle, wave steepness, wave height to depth ratio) are expressly taken into account.

The graph indicates that, irrespective of ξ, wave breaking does not occur if the value of L_{TP} is low. This means that below a given bound, which is actually unknown at this stage of the research, the thrust at the toe of the *focuser* is unable to impress to the fluid a variation of momentum such to drive waves to collapse.

In the picture, this "critical threshold" has been tentatively represented by the black solid curve of equation:

$$L_{TP} = \frac{0.021\,\xi}{1+0.031\,\xi} \tag{6}$$

which tends to 0 for small values of the Iribarren number, as on very mild slopes the waves are always expected to break. On the other hand, the limit of Eq. (6) for $\xi \to \infty$ is 0.68, which represents the shallow water approximation of the Daniel's criterion (1952) for the onset of breaking at vertical face breakwaters:

$$\frac{H}{d} \equiv (L_{TP})_{shall.} = 0.68 \tag{7}$$

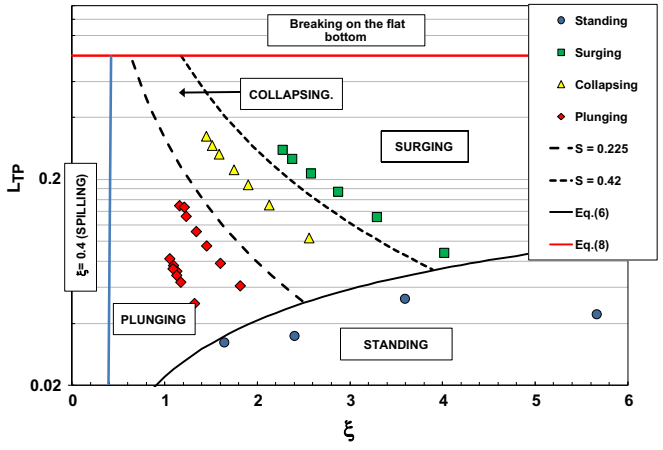

Fig. 20. *The plane ξ, L_{TP}.*

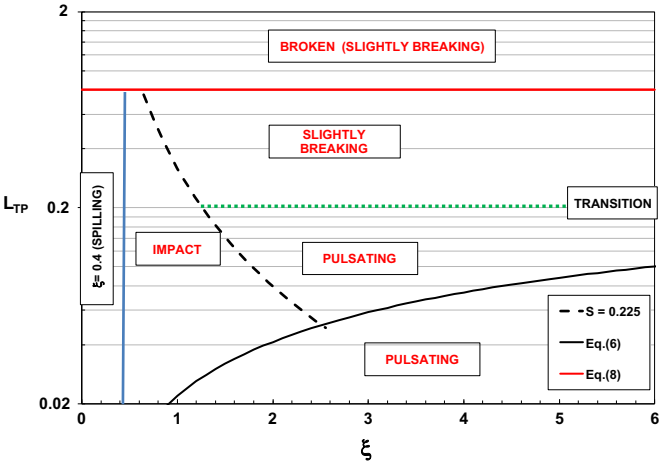

Fig. 21. Tentative map for loading cases at SSGs.

Once wave breaking has taken place, the wave shapes are actually better distinguished via the mean slope parameter *S*., rather than through the Iribarren number. In other words, the breaker types seem more sensitive to a change in the relative water depth compared to the wave steepness. $S=0.420$ and $S=0.225$ are proposed as preliminary limits for the transitions from surging to collapsing and from collapsing to plunging.

An interesting consequence of the above result is that, for a given value of ξ, an increase of thrust may lead to a variation of the breaker shape from plunging towards surging, meaning that the phase of the wave at the incipient breaking is moving back from the crest to the trough (run-down). This would corroborate the reasoning of Hughes (2004), who claimed that being the Iribarren number the same, the features of breakers may change depending on the wave height to depth ratio at the toe of the slope.

The graph of Fig. 20 is completed by the spilling breaker bound suggested by Battjes (1974) in terms of inshore Iribarren number ($\xi=0.4$), and by a shallow water limit for the initiation of breaking on the flat bottom:

$$\frac{H}{d} \equiv (L_{TP})_{shall.} = 0.8 \tag{8}$$

The plane (ξ, L_{TP}) can also be used to predict the different loading cases. Based on the results discussed above, three main zones may be distinguished, namely a *pulsating area* below the curve of Eq. (6), an *impact area* coinciding with the "plunging zone" of Fig. 20 and a *transition domain* (Fig. 21). Within the latter, the forces can be either *pulsating* or *slightly breaking*, depending on whether L_{TP} is lower or larger than 0.2. Finally, the Eq. (8) may be interpreted as the lower bound of a zone where the *broken waves* are expected to produce *slightly breaking* forces.

6. Prediction of wave loadings at the front face of the structure.

In the earlier studies (Vicinanza and Frigaard, 2009; Vicinanza et al., 2011; Buccino et al., 2012), the authors have considered the possibility of predicting the forces exerted by waves on *SSGs* using the equations of the Japanese design practice for monolithic sloping face breakwaters. (Takahashi et al., 1994; Tanimoto and Kimura, 1985). To this purpose, the ensemble "*SSG+focuser*" has been treated as a unique rigid body subjected to the action of waves.

Despite that approach has led, in some cases, to a reasonable agreement with the experimental data, it should be noticed that the prediction formulae employed:

1. have an essentially deterministic nature and do not allow accounting for the inherent variability affecting the loading process even under regular waves;
2. are basically valid for "non-impact" wave conditions;
3. give no information on the rise-time of the wave force, which might be important when a dynamic analysis of the structure response is carried out.

For these reasons a novel method is presented below, where the wave pressures and the corresponding rise times, under both impact and non impact conditions, are thought as random variables of assigned distribution; in this way the variability induced by the randomness of breaking (for given *H* and *T*) can be modeled. Obviously, the variance of the probability density functions (*pdf*) will tend to zero as soon as the loading process becomes repeatable.

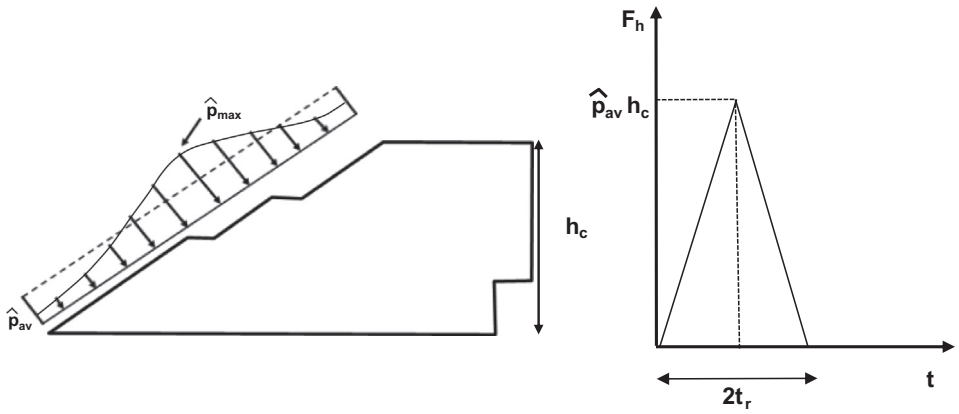

Fig. 22. Simplified loading scheme.

6.1. General assumptions and simplifications

At the instant of force peak, the pressures distribution onto the front face of the device is assumed uniform, with a magnitude, $\hat{p}_{av.}$, equal to the average pressure along the wall (Fig. 22, left part). The latter has been calculated dividing the peak of the horizontal component of F_{int} (e.g. Figs. 14 and 16) by the height of the WEC, h_c. The single force events are approximated to triangular pulses of duration equal to twice the measured rise time t_r (Fig. 22, right part).

The results of previous sections indicate that a rectangular distribution of pressures leads to a realistic estimate of the force application point for non-impacting waves with significant overtopping, which is the most frequent design situation; in the other cases this assumption is cautious, as it wreaks an over-prediction of the overturning moment about the structure heel.

Along with the mean value, in the following also the maximum of the pressure distribution, $\hat{p}_{max}$, is considered; this quantity, not dealt with in the previous research, is central to assess the thickness of the outer plates of *SSG*.

The location of $\hat{p}_{max}$ has to be individuated necessarily on statistical basis, since it has been seen that under the same regular wave train the distribution of loadings may change from event to event (Fig. 15).

Here we assume this position coincides with that of the transducer where the *maximum modal value of the peak pressure* ($\hat{p}$) has been recorded. The mode has been estimated from the histogram of $\hat{p}$ (e.g. Fig. 17), using a number of bins in accordance with the Stegun's rule. Obviously, the extrapolated values at the ends of the wall (top and toe) have been not considered in this phase.

6.2. The joint probability distribution of $\hat{p}_{av.}$ and t_r

It has been observed that for a given wave height and period, the joint probability density function (*j-pdf*) of $\hat{p}_{av.}$ and t_r can be reasonably assumed to be a bivariate log-normal. The distribution can be written as:

$$f(\boldsymbol{X}) = |2\pi\Sigma|^{-0.5} exp\left\{-\tfrac{1}{2}(\boldsymbol{X}-\boldsymbol{\mu})^t \Sigma^{-1}(\boldsymbol{X}-\boldsymbol{\mu})\right\} \tag{9}$$

in which $\mathbf{X}$ is the vector of the "log-variables", $\boldsymbol{\mu}$ is the vector of averages and Σ is the matrix of covariance. Here we set:

$$\boldsymbol{X} = (X_1, X_2) = \left[ln\left(\frac{\hat{p}_{av.}}{\rho g d}\right), ln\left(\frac{t_r}{T}\right)\right] \tag{9a}$$

$$\boldsymbol{\mu} = \left(\mu_{X_1}, \mu_{X_2}\right) \tag{9b}$$

$$\Sigma = \begin{pmatrix} \sigma_{X_1}^2 & r\sigma_{X_1}\sigma_{X_2} \\ r\sigma_{X_2}\sigma_{X_1} & \sigma_{X_2}^2 \end{pmatrix} \tag{9c}$$

where μ_{Xi} and σ_{Xi} represent the mean and standard deviation of the marginals and r is the correlation coefficient.

In the examples displayed in Figs. 23 and 24, the top panels (*a* and *b*) report the Q-Q plots of the variables X_1 and X_2; this to show the marginals are *individually* Gaussian (necessary but not sufficient condition to the bivariate normality).

Then, the Chi-square probability plot of the *sample values* of the quantity $(\boldsymbol{X}-\boldsymbol{\mu})^t \Sigma^{-1}(\boldsymbol{X}-\boldsymbol{\mu})$ is given in the panel *c*, to demonstrate that X_1 and X_2 are also *jointly* normal; it has been argued by Johnson and Wichern (1998) that in a bivariate normal random vector, the quantity above has a chi-square probability distribution with 2 degrees of freedom. Thus, if the points in panel *c* tend to fall along a straight line, our hypothesis cannot be rejected.

The figures are completed with the confidence ellipse of equation:

$$(\boldsymbol{X}-\boldsymbol{\mu})^t \Sigma^{-1}(\boldsymbol{X}-\boldsymbol{\mu}) = \chi_2^2(0.05) \tag{10}$$

which should contain approximately the 95% of data (panel *d*), and with a 3D view of the fitted bivariate surface (panel *e*), along with its contour-lines (panel *f*).

6.3. The probability density function of $\hat{p}_{max.}$

Analogously to $\hat{p}_{av.}$, also the maximum peak pressure can be reasonably described through a log-normal distribution. Fig. 25 shows four examples of Q–Q plot of the variable $ln(\hat{p}_{max.}/\rho g d)$; each panel corresponds to a different wave shape, i.e. quasi-standing, surging, collapsing and plunging. From the graph one can easily realize how the variance of the loading process increases passing from quasi-standing waves to plunging breakers.

It is worth noticing that in both the present and the previous paragraph, the log-normal distribution is used for all the variables under both impact and non impact conditions; this represents in fact a generalization of the approach employed by Fuhrboter (1985), Kirkgoz (1995), Vicinanza (1997), Calabrese et al. (2000) and many others, where such a *pdf* was fitted only to the impulsive peak pressures.

After establishing the probabilistic models, the problem boils down to the estimation of parameters. Overall they are seven, namely the mean and standard deviation of $\hat{p}_{av}$ and t_r (4 parameters), their correlation coefficient (r) and the mean and standard deviation of $\hat{p}_{max.}$

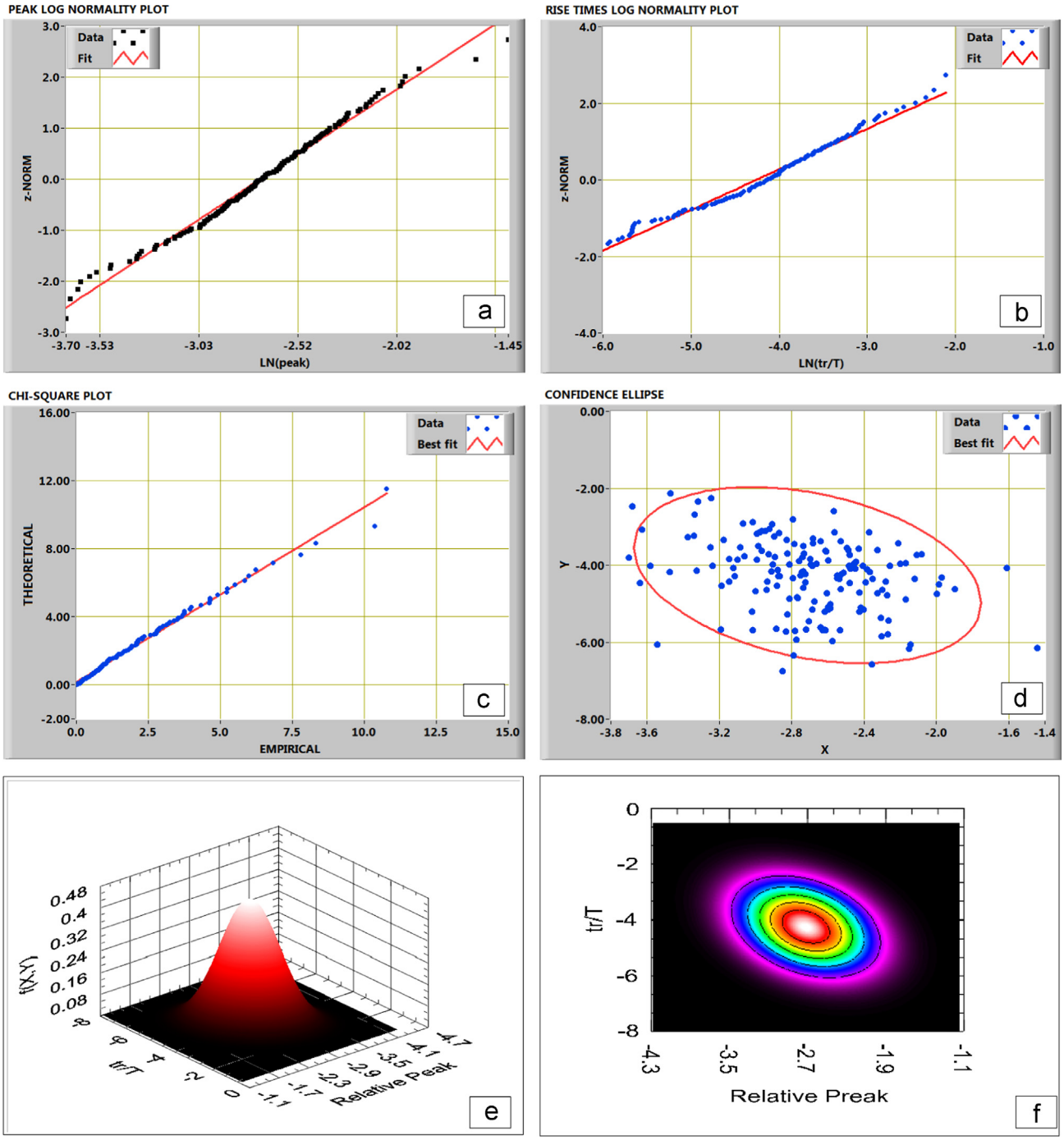

Fig. 23. Bivariate log-normal plots for $H=0.113$ m, $T=0.8$ s (plunging breaker). (a) the log-normal plot for $\ln(\hat{p}_{av.}/\rho g d)$; (b) the log-normal plot for $\ln(t_{r.}/T)$; (c) the Chi-square probability plot of the sample values of the quantity $(X-\mu)^t\Sigma^{-1}(X-\mu)$;(d) the confidence ellipse; (e) 3D view of the fitted bivariate surface; (f) contour-lines of the curve.

In the next paragraphs, a set of equations are proposed, where those quantities are predicted in function of the governing variables introduced in Section 5.

6.4. *The mean of* $\hat{p}_{av}$

Under non-impact conditions a crude predictive model has been developed, which employs an approach conceptually similar to that used by Tanimoto and Kimura (1985) for trapezoidal walls. Assuming that the device and the steep foreshore behave like a unique structure (Fig. 26), from the conservation of the horizontal momentum follows that the maximum horizontal momentum flux of the incoming waves at the toe of the focuser (M_F) should equal the horizontal component of the peak force exerted onto the structure (Π_x). Under the hypothesis of uniform distribution of pressures we have:

$$\Pi_x = \hat{p}_{av.}(d+R_c) = M_F \tag{11}$$

Now we linearize the previous equation retaining only the pressure term in M_F (see Eq. (3)) and noting that in the case of *SSG*s it can be assumed that R_c is of the order O(H); accordingly, the product $(\hat{p}_{av.}\, R_c)$ is of order $O\left(H^2\right)$ and can be neglected.

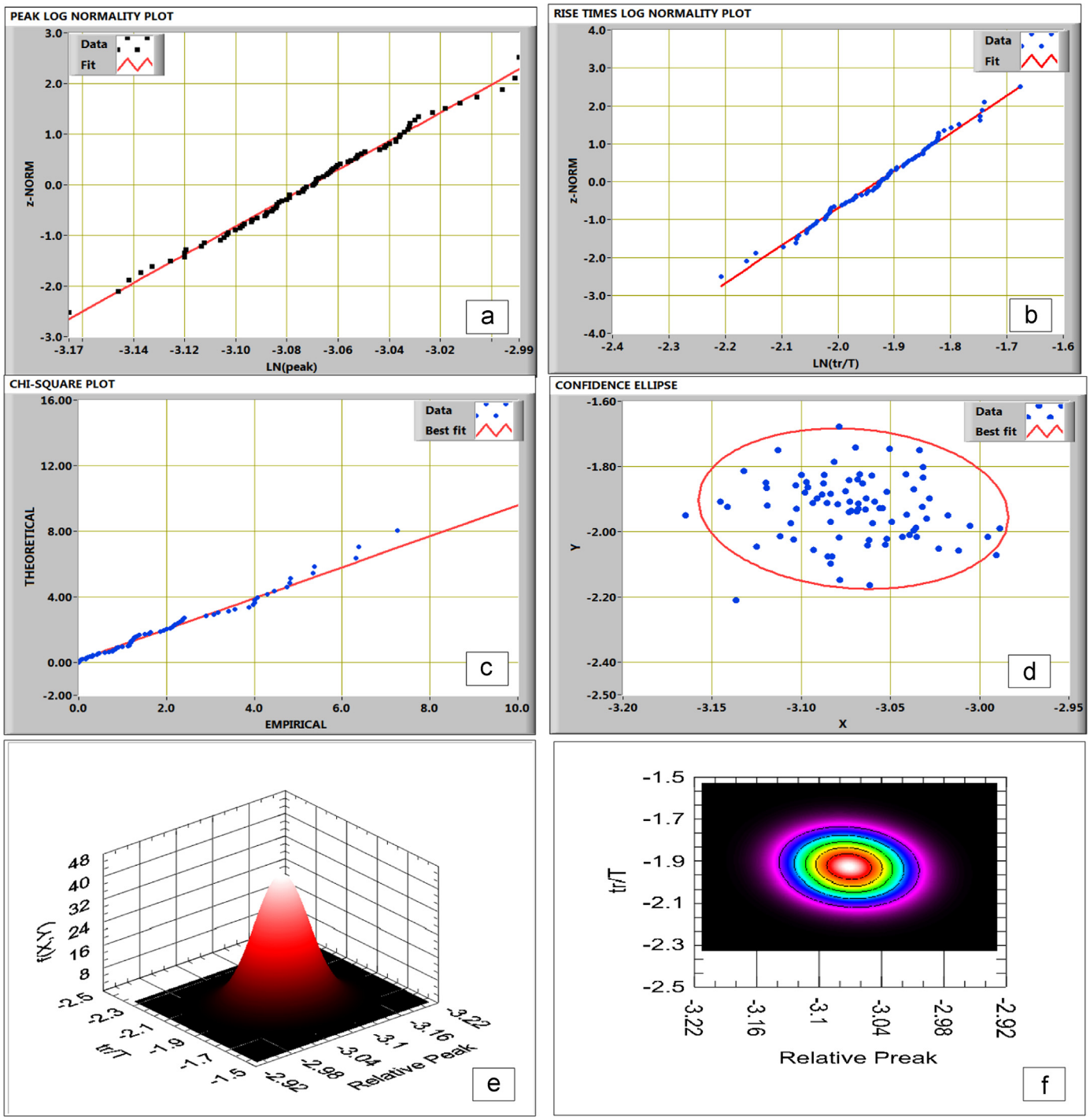

Fig. 24. Bivariate log-normal plots for $H=0.128$ m, $T=1.5$ s (collapsing-breaker). (a) the log-normal plot for $\ln(\hat{p}_{av.}/\rho g d)$; (b) the log-normal plot for$\ln(t_{r.}/T)$; (c) the Chi-square probability plot of the sample values of the quantity $(X-\mu)^t\Sigma^{-1}(X-\mu)$;(d) the confidence ellipse; (e) 3D view of the fitted bivariate surface; (f) contour-lines of the curve.

Thus, after taking the average over a given experiment we obtain:

$$E(\hat{p}_{av.}) = \frac{M_F}{d} = \rho g \frac{H}{2}\frac{\tanh(kd)}{kd} \tag{11b}$$

In which $E(^\circ)$ represents the expectation operator. The latter does not appear at the right hand side of Eq. (11b), since, oppositely to the wave pressure, the variance of H and T within the same regular wave train can be neglected. After dividing both sides by $\rho g d$ one finally gets:

$$E\left(\frac{\hat{p}_{av.}}{\rho g d}\right) = \frac{1}{2} L_{TP} \tag{12}$$

or more generally:

$$E\left(\frac{\hat{p}_{av.}}{\rho g d}\right) = m\, L_{TP} \tag{12b}$$

where the coefficient m accounts for the main terms neglected in the balance, namely wave reflection, inertia forces and loss of momentum

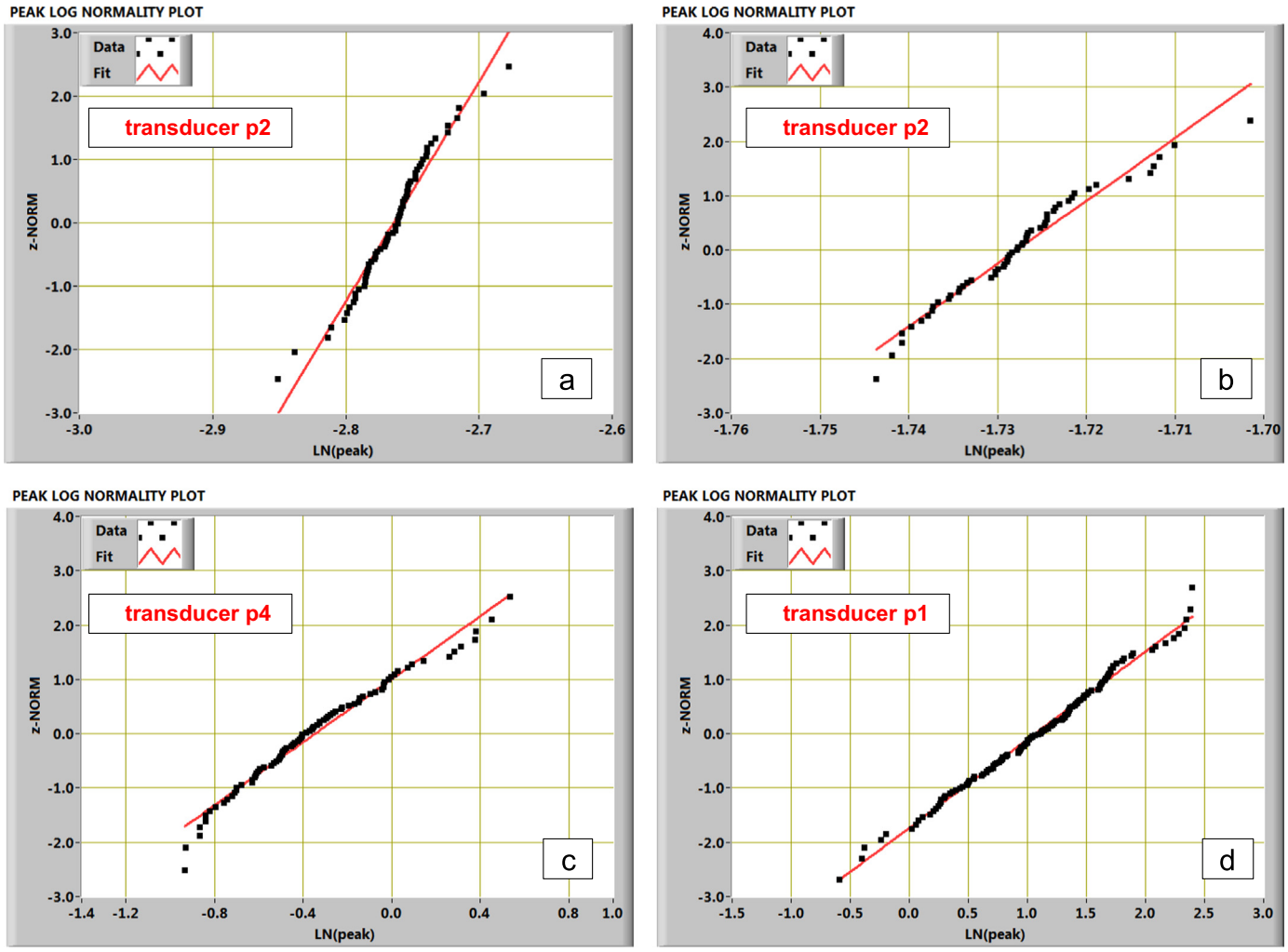

Fig. 25. *Q-Q normal plots for* $\ln(\hat{p}_{max}/\rho gd)$. Panel (a): $H=0.049$ m, $T=0.8$ s (quasi-standing wave); (b): $H=0.076$ m, $T=2$ s (surging breaker); (c) $H=0.198$ m, $T=1.5$ s (collapsing breaker); (d) $H=0.147$ m, $T=1$ s (plunging breaker).

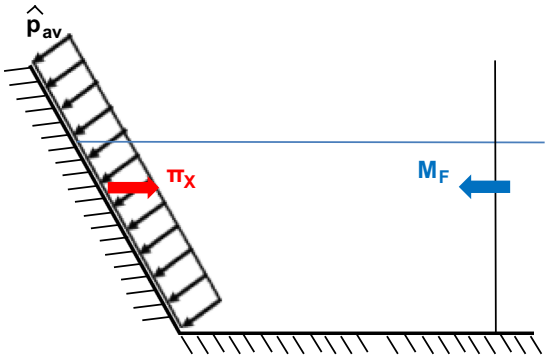

Fig. 26. *Calculation scheme for* $E\left(\frac{\hat{p}_{av}}{\rho gd}\right)$.

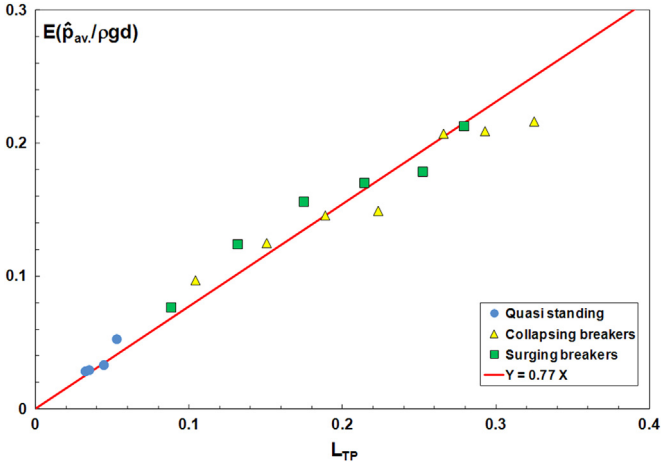

Fig. 27. Expected non-dimensional mean pressure vs. L_{TP} (non impact waves).

flux by overtopping. In theory the value of m should not exceed 1, which corresponds to the case of a non-overtopped vertical wall understanding waves.

From the comparison with data (Fig. 27), a best fit value of $m=0.77$ has been estimated, which is consistent with the expectations.

The R^2 statistics exceeds 0.95, indicating a satisfactory prediction power. The standard error s_e (standard deviation of residuals) equals 0.015. Yet, the graph seems to suggest that the model might suffer from a small non linearity (curvature of data); given the high value of the correlation index and the small residual error, this effect can be of course neglected for values of L_{TP} within the range of the present data set (0.03–0.32), but needs to be accurately checked outside of it.

Under impact waves, the loading process becomes highly non-linear and the coefficient m in the Eq. (12b) can be considered no longer constant; beside the wave momentum flux (pressure forces), a central role is now expected to be played by the inertia forces

which, according to the linear wave theory, are proportional to the wave steepness. For this reason m is supposed to be a decreasing function of the Iribarren number, which can be roughly viewed as the ratio between the along-slope components of the gravity forces (representing a resistance to the wave motion) and the inertia forces. The following expression is proposed:

$$E\left(\frac{\hat{p}_{av.}}{\rho g d}\right) = \left[2.68\,\xi^{-2.42}\right] L_{TP} \tag{13}$$

with $R^2=0.90$ and $s_e=0.025$. Caution is recommended in using the above formula outside the range:

$$0.015 \le \xi^{-2.42} L_{TP} \le 0.108 \tag{13b}$$

Fig. 28 shows the comparison between calculated and measured value of $E(\hat{p}_{av.}/\rho g d)$

6.5. The standard deviation of $\hat{p}_{av}$

The standard deviation of the non-dimensional mean pressure is significantly influenced by the Iribarren number. Fig. 29 clearly shows a decrease of variability with increasing ξ, so that the loading process can be considered practically repeatable beyond the Iribarren and Nogales (1949) breaking limit $\xi=2.3$. According to Battjes (1974), the latter tends in fact to separate a zone of complete breaking (high variability) from a zone about halfway between breaking and reflection (quasi-standing waves and surging breakers with low variability of $\hat{p}_{av}$).

However, for a given ξ the occurrence and intensity of wave breaking have been seen to be also affected by the linear thrust parameter L_{TP}; as the latter increases, the waves pass first from non-breaking to breaking and once the rupture has taken place, the scales of dissipation tend to progressively increase. This definitely leads the variance of the process to raise.

Then, for a more effective prediction, the following equations are suggested:

$$\sqrt{VAR\left(\frac{\hat{p}_{av}}{\rho g d}\right)} = \begin{cases} 0.0012 + 0.0474\,u + 0.8017\,u^2 & (\textit{non impact waves } R^2 = 0.93\ ) \\ 0.0009\exp(10.39\,t) & (\textit{impact waves } R^2 = 0.89) \end{cases} \tag{14}$$

where:

$$\begin{cases} u = \frac{L_{TP}}{\xi^{0.6}} \\ t = \frac{L_{TP}^{0.3}}{\xi} \end{cases} \tag{15}$$

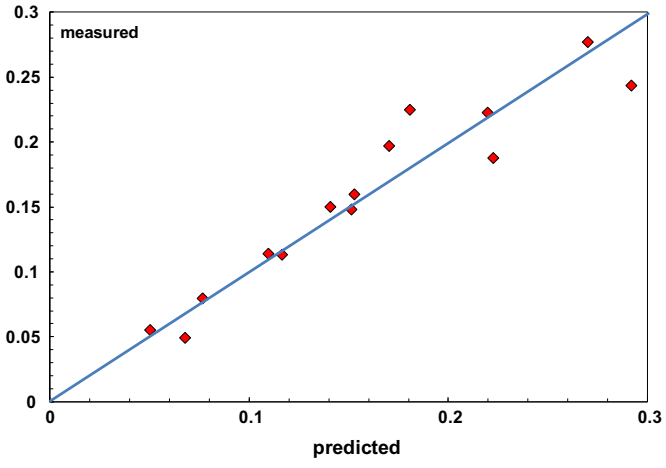

Fig. 28. *Measured vs. predicted* $E\left(\frac{\hat{p}_{av}}{\rho g d}\right)$ *for impact waves.*

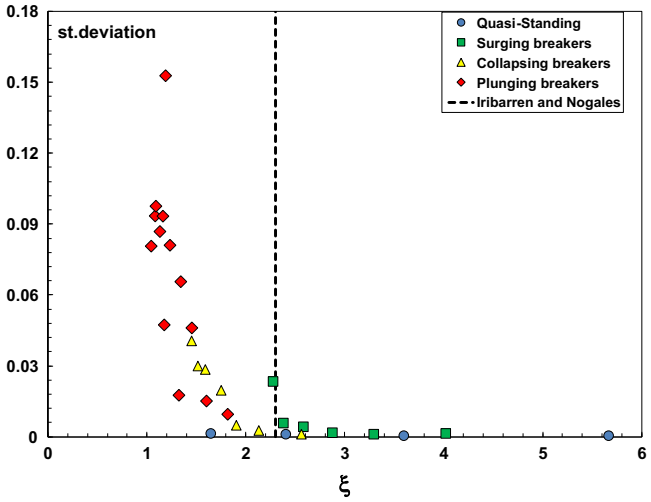

Fig. 29. Standard deviation of $\left(\frac{\hat{p}_{av}}{\rho g d}\right)$ vs. the Iribarren number.

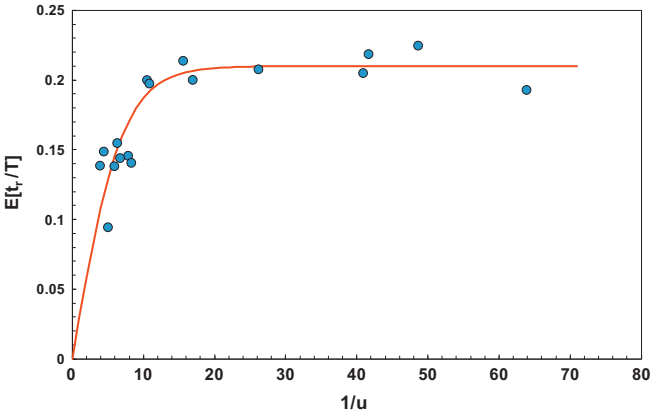

Fig. 30. Mean of the non-dimensional force rise-time vs. Eq. (17). Non impact waves.

The standard error is respectively 0.013 and 0.026.

Eq. (14) indicates that the Iribarren number is the most important parameter under impact conditions, whereas L_{TP} dominates under non impacting waves. The application ranges of the formulae are:

$$\begin{cases} 0.0157 \le u \le 0.2600 \\ 0.2407 \le t \le 0.4933 \end{cases} \tag{16}$$

6.6. The non dimensional rise time t_r/T

Under non impact conditions, the average of the marginal *pdf* of the force rise time to wave period ratio can be estimated as (Fig. 30):

$$E\left[\frac{t_r}{T}\right] = 0.21\ tanh\left(\frac{\pi}{22\,u}\right) \quad \left(R^2 = 0.80 s_e = 0.019\right) \tag{17}$$

As expected, Eq. (17) tends to 0.21 (theoretical value for sine waves) as the Iribarren number grows and/or the momentum flux decreases.

On the other hand, for impact conditions the following relationship has been found (Fig. 31):

$$E\left[\frac{t_r}{T}\right] = 0.023\xi^{2.94} \quad \left(R^2 = 0.86\ s_e = 0.009;\ 1 \le \xi \le 1.85\right) \tag{18}$$

As far as the standard deviations are concerned, the following approximate equations may be used:

$$\sqrt{VAR\left(\frac{t_r}{T}\right)} = \begin{cases} 0.011\ exp[6.09\ u] & \left(non\ impact\ waves,\ R^2 = 0.53\ s_e = 0.0124\right) \\ 1.14\ \mathrm{E}\left(\frac{t_r}{T}\right) & (impact\ waves) \end{cases} \tag{19}$$

The second of the above formulae simply states that the marginal *pdf* of the non dimensional rise-time of the wave force has a 114% variation coefficient under impact events. This does underline the extreme instability of this kind of phenomenon.

It could be finally useful to remark that the Eq. (17) and the first of the Eq. (19) are valid in the range defined by the first of the Eq. (16).

6.7. The linear correlation coefficient, r

The linear correlation coefficient, which links X_1 and X_2 in Eq. (9a), can be crudely estimated as follows:

$$r = \begin{cases} 0.025 (quasi-standing\ waves,\ s_e = 0.12) \\ 0.662\ ln\xi - 0.505\ (breaking\ waves,\ R^2 = 0.73\ s_e = 0.15) \end{cases} \tag{20}$$

The second of the previous formulae holds for values of the Iribarren number included between 1 and 4.

It should be noticed that for plunging breakers, corresponding to low values of ξ, the correlation coefficient becomes rather negative (around −0.45). This because, as argued by a number of authors (e.g. Bagnold, 1939; Hattori and Arami, 1992), the impulse of wave loadings tends to conserve oneself under impact conditions. On the other hand, force and rise-time seem nearly uncorrelated under non-breaking waves, such that their joint *pdf* tends to the simple product of the marginals.

6.8. Mean and variance of the maximum pressure $\hat{p}_{max}$

Under non impact conditions, the use of the simple linear relationship of Eq. (12b) revealed itself effective only for large L_{TP}s, say beyond 0.15. For smaller values, a non-linear term has to be introduced. Thus, the following predictive model is proposed:

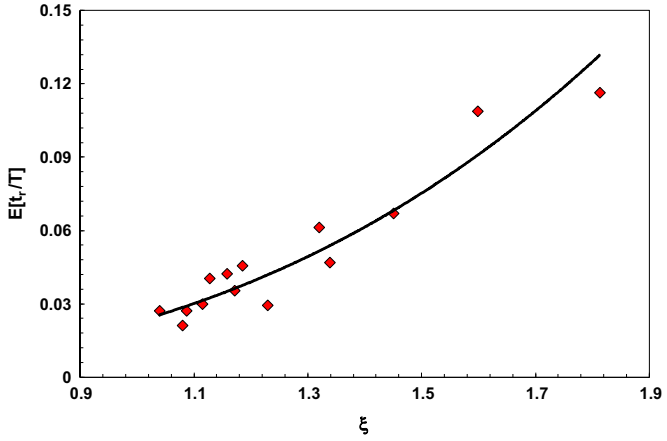

Fig. 31. Mean of the non-dimensional force rise-time vs. Eq. (18). Impact waves.

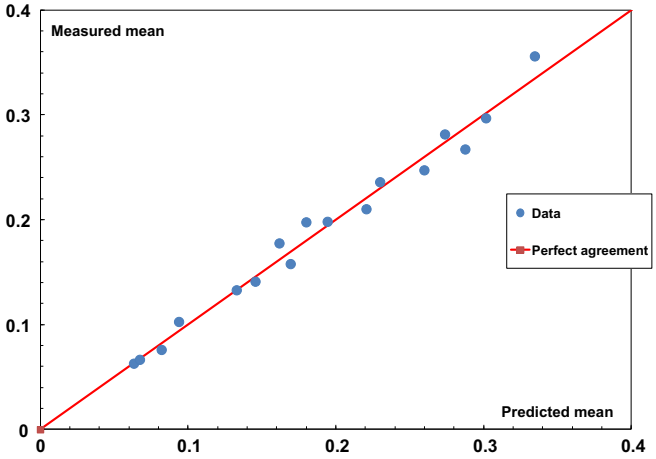

Fig. 32. Measured vs. predicted $E\left(\frac{\hat{p}_{max}}{\rho g d}\right)$ for non impact waves.

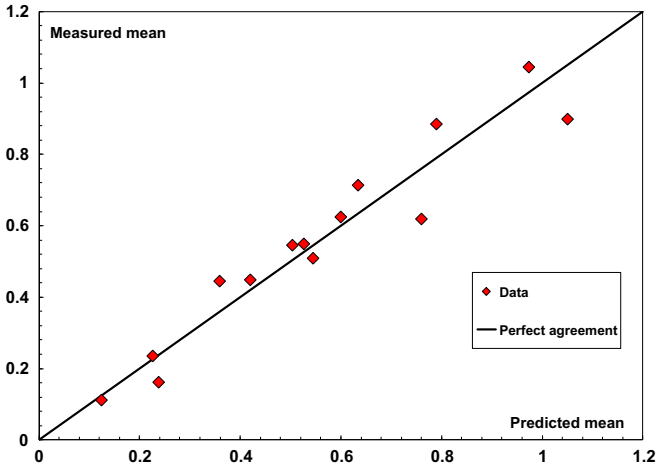

Fig. 33. Measured vs. predicted $E\left(\frac{\hat{p}_{max}}{\rho g d}\right)$ for impact waves.

$$E\left(\frac{\hat{p}_{\max}}{\rho g d}\right) = \begin{cases} m\ L_{TP} \\ m = \max[2.275\ \exp(-4.68\ L_{TP}); 1.03] \end{cases} \tag{21}$$

which, as shown in Fig. 32, leads to an excellent agreement with data (R^2=0.98, s_e=0.011).

Under plunging breakers, the factor *m* is again assumed to be a decreasing function of the Iribarren number. This led to (Fig. 33):

$$E\left(\frac{\hat{p}_{\max}}{\rho g d}\right) = \left[10.19\xi^{-2.77}\right] L_{TP} \quad \left(R^2 = 0.92; s_e = 0.082\right) \tag{22}$$

which should be cautiously used within the range:

$$0.012 \le \xi^{-2.77} L_{TP} \le 0.103 \tag{22b}$$

As far as the standard deviations are concerned, the following expressions are suggested:

$$\sqrt{VAR\left(\frac{\hat{p}_{\max}}{\rho g d}\right)} = \begin{cases} \max[0.095\ t; 0.352t - 0.084\ ] & \left(non\ impact\ waves\ R^2 = 0.95\right) \\ 0.0046\exp(9.98\ t) & \left(impact\ waves\ R^2 = 0.88\right) \end{cases} \tag{23}$$

with a standard error of respectively 0.007 (non impact) and 0.093 (impact).

Compared to the case of the average pressure (Eq. 14), the formula for non impacting waves is now dependent on the variable t, rather than on u. This indicates a larger influence of the Iribarren number.

Eq. (23) hold for t ranging in the interval 0.0693–0.4933. It is finally important to point out that, similarly to the case of $\hat{p}_{av.}$, the variance of the process can be neglected when ξ overcomes the limit of 2.3.

6.9. *Tentative estimation of sampling and scale effects for impact loadings.*

Besides the inherent variability of pressures and rise times, which is rather high, impact loadings are affected by supplementary uncertainties, related to a number of phenomena which render difficult the transfer of results from laboratory to real situations. Very important examples are the effects of the rate of sampling of the pressure signals and of the model scale. To include them in the predictive scheme discussed in the paragraphs above, the equations for calculating the mean and the variance of $\hat{p}_{av.}$, $\hat{p}_{max.}$ and t_r, should be multiplied by two coefficients, say $C_{samp.}$ and C_{scale}, the value of which is not easily assessed. However, an order of magnitude estimate is attempted below; given the lack of studies on the specific case of *SSGs*, the analysis is based on the research carried out on vertical breakwaters.

Regarding the sampling effect, Oumeraci et al. (1994) found out that at a frequency of 1 kHz nearly the 20% of the *maximum peak pressure* ($\hat{p}_{max.}$) was lost, whereas the *peak force amplitude* (and then $\hat{p}_{av.}$), was reduced by nearly 10%. These results have been recently confirmed by Marzeddu and Gironella (2013), who sampled pressure signals up to 19,500 Hz and estimated a drop of about 21% on the maximum pressure and of 14% on the force peak. As far as the rise times are concerned, no direct indications have been given. However, since Oumeraci et al. (1994) observed no loss of impulse at 1000 Hz, it can be reasonably assumed that the correction factor for t_r is the reciprocal of that associated with $\hat{p}_{av.}$

Scale effects on impact loadings arise from the presence of a significant volume fraction of air, which greatly increases the compressibility of water. This has the effect of cushioning the most violent events, leading to a reduction of the scaling factors compared to the simple Froude's law. Despite many scientific reviews have focused on this topic (e.g. Bullock et al., 2001) the indications for practical applications are actually very few.

After comparing the results of field measurements with those of laboratory tests, Allsop et al. (1996) proposed a reduction factor for $\hat{p}_{max.}$ included between 0.40 and 0.45, whereas the rise times were suggested to increase by a factor ranging from 4 to 7.

A more rigorous method has been recently suggested by Cuomo et al. (2010), based on the so-called Bagnold-Mitsuyasu similitude. The approach uses an analogy between water waves impinging a vertical wall and a water hammer compressing air in a piston.

The first step is calculating the Bagnold number for *both the model and the prototype*:

$$Bgn = \frac{\rho K_w u_0^2}{p_0 D} \tag{24}$$

where ρ is the water density, K_w is the thickness of water mass effectively contributing to the impact, u_0 is the velocity of the water hammer, which equals the wave crest celerity, p_0 is the atmospheric pressure and D is the mean thickness of the air pocket trapped by the plunging breaker against the wall (see Fig. 18).

According to the authors suggestions, the above quantities have been estimated as follows:

$$\begin{cases} u_0 = \sqrt{g(d+H)} \\ D = \frac{\pi}{12} H \\ K_w = 0.2\left(1 - \frac{\pi}{12}\right) H \end{cases} \tag{25}$$

As far as ρ is concerned, 1000 has been used for the model (freshwater) and 1033 kg/m^3 for the prototype (saltwater).

As second step, the Takahashi et al. (1985) equation is employed to calculate the expected maximum pressure relative to p_0:

$$Bgn = 5\left(\frac{p_{max}}{p_0}\right)^{2/7} + 2\left(\frac{p_{max}}{p_0}\right)^{-5/7} - 7 \tag{26}$$

After achieving the values of p_{max}/p_0 in the model and in the prototype, the correction coefficient for pressures and forces, C_{scale}, can be estimated as:

$$C_{scale} = \frac{1}{\lambda_F}\left[\frac{\left(\frac{p_{max}}{p_0}\right)_{Prot.} - 1}{\left(\frac{p_{max}}{p_0}\right)_{mod.} - 1}\right] = \frac{\lambda_S}{\lambda_F} \tag{27}$$

in which λ_F is the prototype to model length-scale ratio. It is worth to mention that C_{scale} could be further reduced taking into account of the pressure drop due to the air leakage during the impact event. Although Cuomo et al. (2010) included this effect in their method, it has been cautiously neglected in the present calculations.

Like for the case of sampling effects, the rise time is finally corrected by the reciprocal of Eq. (27).

The values of $C_{samp.}$ and C_{scale} are summarized in Table 3. Overall they lead to reduce the magnitude of pressures by a factor included between 1/4 and 1/5, with a consequent increase of the rise-times.

Combining these results to the experimental indication that the SSG characteristics (mild front slope and shallow water at the toe) may structurally lower the probability of severe impacts, it might be concluded that impulsive loadings are of a little concern for the design of such kind of structures. Of course this preliminary conclusion deserves to be accurately verified through new experimental campaigns to be conducted both in field and in lab. In particular, the effect of different geometries of the foreshore on the breaker shape at the wall needs to be checked.

7. Application to random waves

The most convincing way to apply the results of previous sections to a random wave train is using a "wave by wave approach". Once the design sea-state has been defined through a series of wave heights and periods, employing for example the *j-pdf* suggested by Longuet-Higgins (1975), the individual values of ξ and L_{TP} can be calculated. Thus, a set of points can be plotted on the maps of Figs. 20 and 21, to assess the characteristics of the wave profiles and the nature of loadings exerted on the device. Obviously, the most important information achievable at this stage

Table 3
Correction factors for impact loadings.

Variable	Eqs. to be corrected	C_{sample}	C_{scale} (mean)	C_{scale} (min)	C_{scale} (max)
$\frac{\hat{p}_{av.}}{\rho g d}$	(13)–(14)[a]	1.14	0.21	0.18	0.23
$\frac{\hat{p}_{max.}}{\rho g d}$	(22)–(23)[a]	1.23	0.21	0.18	0.23
$\frac{t_r}{T}$	(18)–(19)[a]	0.88	4.87	4.41	5.49

[a] Only the "impulsive part" needs to be corrected.

is the expected number of plunging breakers, which should be as low as possible to avoid the project to be affected by a significant degree of uncertainty.

Then, the probability distributions discussed in the Section 6 should be interpreted as *pdf*s conditional to the occurrence of a given wave height and period; in this way, the design probability functions of wave loadings (pressure, force and rise times) can be estimated accounting for the randomness of both the wave parameters (wave height and period) and the breaking process. If the latter source of variability is ignored, the loading variables can be deterministically associated to each wave by using the expected values of Eqs. (12),(13),(17),(18),(21) and (22). The analysis presented above suggests this simplification to be rigorously appropriate when all the waves of the design storm have Iribarren numbers larger than 2.3.

The first (partial) verification of the described procedure is discussed below with reference to the experiments of Vicinanza and Frigaard (2009), which, as of today, represent the sole random wave data-set available.

7.1. Description of experiments

Vicinanza and Frigaard conducted their experiments at the "*Deep 3D wave basin*" of Aalborg University (DK). The facility is 15.7 m long, 8.5 m wide and 1.5 m deep and is provided with a snake-front piston type wavemaker, with a total of ten actuators. The *SSG* was a 1:60 model of the pilot plant of Kvitsøy. The device was 0.097 m high (5.82 m in prototype) and had three outer plates inclined by 35° to the horizontal. The *WEC* has been seated on the top of a *focuser* with a 1:1 slope (rocky cliff), giving a value of $tg\alpha_{av.}$ equal to 0.84. The front plates have been equipped with 9 pressure transducers sampled at 200 Hz.

32 *JONSWAP* driven random sea states were run, divided into two groups: 16 long crested (*2D*) and 16 short crested (*3D*). The spectral significant wave height at the toe of the *focuser*, H_{m0}, varied from 0.042 m to 0.25 m; the peak period, T_p, ranged from 1.03 s to 2.07 s. The duration of the wave attacks was approximately 1000 waves.

Each group of experiments (*2D* and *3D*) included 8 tests with waves perpendicular to the structure (*front waves*) and 8 oblique attacks with an angle of 45° (*side waves*). In the 2D experiments, two water levels at the toe of the cliff were changed, namely $d=0.50$ m and $d=0.53$ m; the former made the *SSG* completely exposed (shoreline device). *3D* tests were instead performed with a unique value of the swl ($d=0.53$ m) and with 2 different exponents of the cos^{2n} spreading function: $n=4$ (large spreading) and $n=10$ (small spreading).

7.2. Limitations and assumptions

Unfortunately the only data available from the above experiments is the significant wave height, the peak period and the spatial distribution of pressures at the peak force $\hat{F}_{1/250}$ (mean of the highest 1/250th peaks of force). No information on the rise-times has been stored, basically because the wave loadings recorded could be considered quasi-static.

Hence, some hypotheses have to be necessarily introduced; we assume the wave elevation process at the toe of the cliff to be very narrow banded in the frequency domain, so that the wave height distribution follows the *Rayleigh pdf* and the periods are all equal to T_p.

It is worth emphasizing that if the little information available limits (significantly) the possibility of verifying the "wave by wave" approach, they ironically give the opportunity of assessing how that procedure might work under the hypotheses most frequently adopted by practical engineers.

7.3. Results of comparison

The first consequence of the hypothesis of narrow banded spectrum is that for these tests all the waves up to $H_{1/250}$ have Iribarren numbers larger than 2.3. This means that the variance of the loading process due to the randomness of breaking can be neglected. Then, since the wave period is assumed constant, we can conclude that the cumulative distribution function (*cdf*) of the wave forces is the same as that of the wave heights; in other words $H_{1/250}$ gives rise to $\hat{F}_{1/250}$, according to the approach followed by Goda (1986) and commonly accepted in the engineering applications.

In Fig. 34 ξ and L_{TP} are calculated with reference to the wave parameters $H_{1/250}=1.8\ H_{m0}$ and T_p.

For sake of clearness only the long-crested wave data is reported in the picture, seeing that the 3D tests have in fact the same coordinates.

Most of points are in the domain of surging breakers, apart from two of them which fall in the quasi-standing zone. This result is in a fair agreement with the visual observations; the pressure patterns recorded (see Fig. 7 of Vicinanza and Frigaard (2009)) are either of the pulsating type or slightly double-peaked, in a qualitative accordance to what described in the Section 4 of this article.

In the two tests with non-breaking waves, the roof of the *WEC* was not overtopped, due to the low value of the wave thrust at the base of the *focuser* compared to the crest freeboard. As for the remaining experiments, the values of $(L_{TP})_{1/250}$ are rather high and produce severe overtopping; the linear thrust parameter reaches the level of 0.76, whereas the maximum measured in the regular wave tests was 0.32. However, no breaking has been observed seaward the cliff and this makes the hypothesis of Rayleigh distribution of the wave heights quite reasonable.

The application of the Eqs. (12b) and (21) is presented in Figs. 35 and 36 where the predicted values of force, overturning moment about the heel and maximum pressure ($\hat{p}_{max.}$) are compared to the measured ones. The 3D data has been not parameterized with respect to n, as no influence of the degree of spreading has been detected (Vicinanza and Frigaard, 2009).

The agreement is rather good and the R^2 statistics exceeds 0.95 in all the three cases. Apart from a single outlier, the maximum relative error is about 20%. The satisfactory prediction of moments seems to confirm that the hypothesis of uniform distribution of pressures may suit to most of the design situations. In this respect it should be noticed that in the low panel of Figure B, the torques are all negative (the values of "$-M$"are in fact reported). This means that the stabilizing effect of the vertical component of the force prevails on the overturning effect of the horizontal one.

The performance of the Eq. (21) is surprisingly good (Fig. 36) bearing in mind the low spatial resolution of the pressure transducers in the regular wave experiments.

The scatter of points in the above graphs is however some larger than what inferred in Section 6; accordingly, the standard error (s_e) of the predictive formulae has to be recalculated. After gathering regular and random wave data (49 experiments on total) s_e resulted 0.026 for the Eqs. (12b) and 0.043 for the formula (21).

Before ending this paragraph, two important issues deserve to be further investigated. The first concerns the possible non linearity of the Eq. (12b), which seemed to arise from the small curvature of the regular wave points in the Fig. 27. To answer this question, in Fig. 37 the residuals $ei_{pav}=(\hat{p}_{av.}/\rho g d)_{meas.}-(\hat{p}_{av.}/\rho g d)_{calc.}$ are plotted vs. the linear thrust parameter for all the available data. The scatter plot exhibits no trend and accordingly the linear relationship of Eq. (12b) can be considered correct with reference to the present data set.

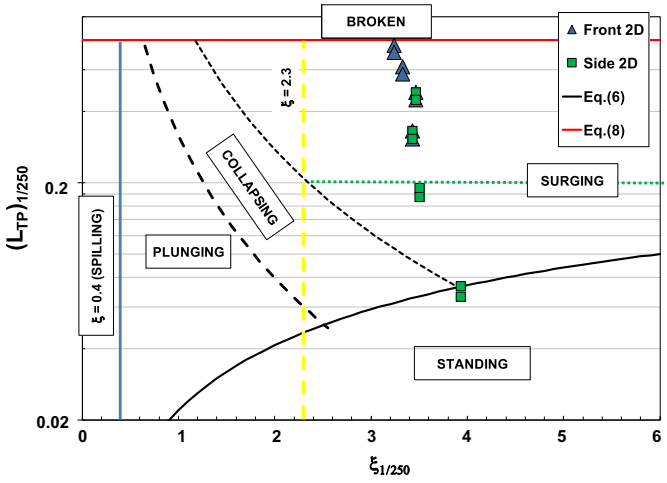

Fig. 34. The tests of Vicinanza and Frigaard (2009) on the map of Figure AA. (2D tets).

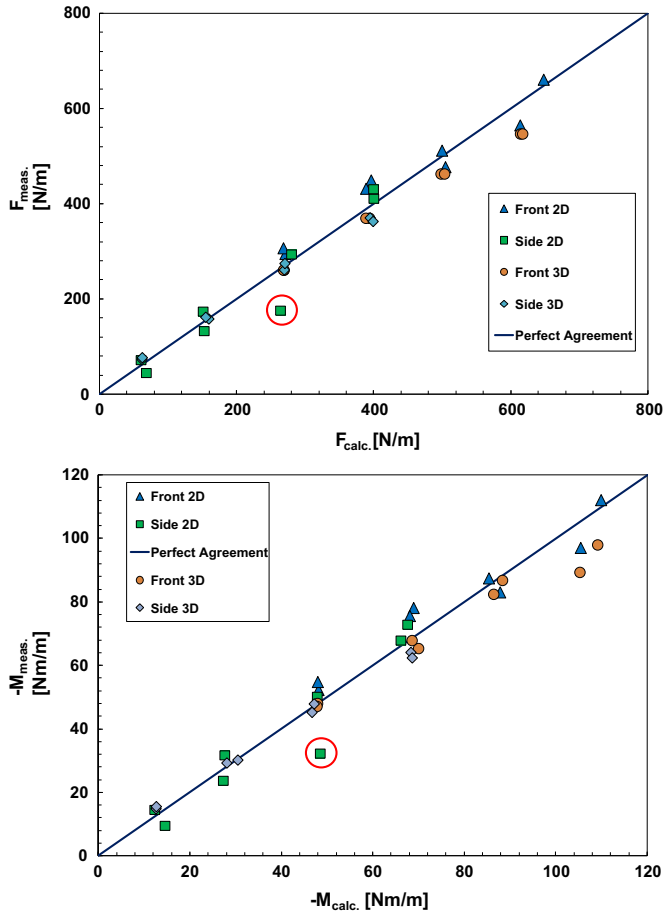

Fig. 35. Eq. (12b) with $m=0.77$ vs. Vicinanza and Frigaard random wave data (2D tests). Top panel: forces; Low panel: moments about the SSG heel.

Yet, it can be observed a certain tendency at underpredicting the *2D* tests and overpredicting the *3D* ones. This is the consequence of the fact that short-crested waves induce loadings slightly smaller, being the wave parameters the same. However, the issue has been considered of little relevance given the very good quality of the estimates.

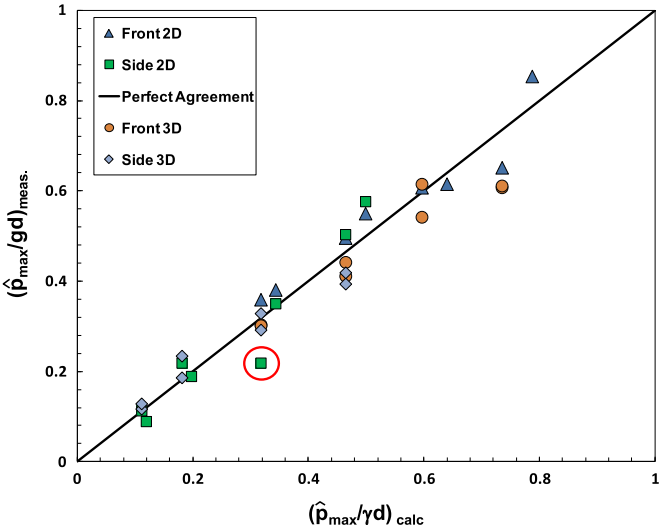

Fig. 36. Measured vs. predicted values of the maximum relative pressure.

The second point of interest is that the Eqs. (12b) and (21) have been applied to both front and side waves, introducing no obliquity correction. From a physical point of view this is consistent, because the wave momentum flux (L_{TP}), which is supposed to generate these non impact loadings, includes only the pressure term and is then independent of the wave direction. To verify the correctness of this assumption, in Fig. 38 the residuals of the non dimensional mean and maximum pressures are plotted against the angle of propagation of waves (random wave tests only). Since again no trend is observed, it can be concluded that the present data set does not contradict the hypothesis formulated.

8. Conclusions

The nature and the magnitude of the actions exerted by waves onto the outer plates of the Seawave Slot-cone Generators (SSG) have been systematically analyzed through a set of regular wave experiments carried out at the Department of Civil, Architectural and Environmental Engineering (DICEA) of the University of Naples *Federico II*. As main outcome of the research, a number of design tools have been suggested, which serve as a guidance for a more rational conceptual design of this kind of device.

The main predictive variables employed in the study are the *surf similarity parameter*, ξ (Eq. (1)), and the *linear thrust parameter*, L_{TP}, which is a linearized slightly modified form of the *wave momentum flux parameter* originally introduced by Hughes (2004). These quantities respectively represent the inertia forces and pressure loads acting at the base of the steep foreshore (*focuser*) at the top of which the *SSG* is usually located.

In Section 5, it has been seen the plane (ξ, L_{TP}) can be effectively used to discriminate among the different wave profiles and loading cases occurring at the wall (Figs. 20 and 21). Although the few data available in the present study does not allow to define with sufficient precision the bounds of the different zones, this kind of representation appears very promising, since all the variables affecting the wave-structure interaction (slope angle, wave steepness, wave height to depth ratio) are expressly taken into account. However, the verification of the predictive maps against the random wave data of Vicinanza and Frigaard (2009) has resulted rather favorable (Fig. 34).

Since the occurrence of breaking impresses a significant variability to the loading process, a probabilistic approach has been used to predict the mean and maximum wave pressures onto the

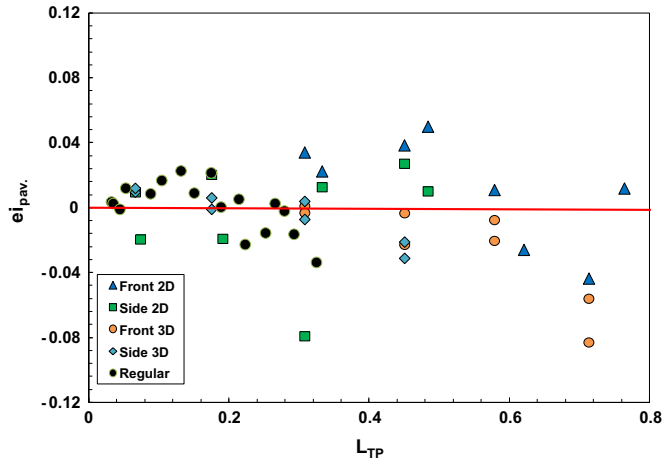

Fig. 37. Residuals the Eq. (12b) vs. L_{TP}.

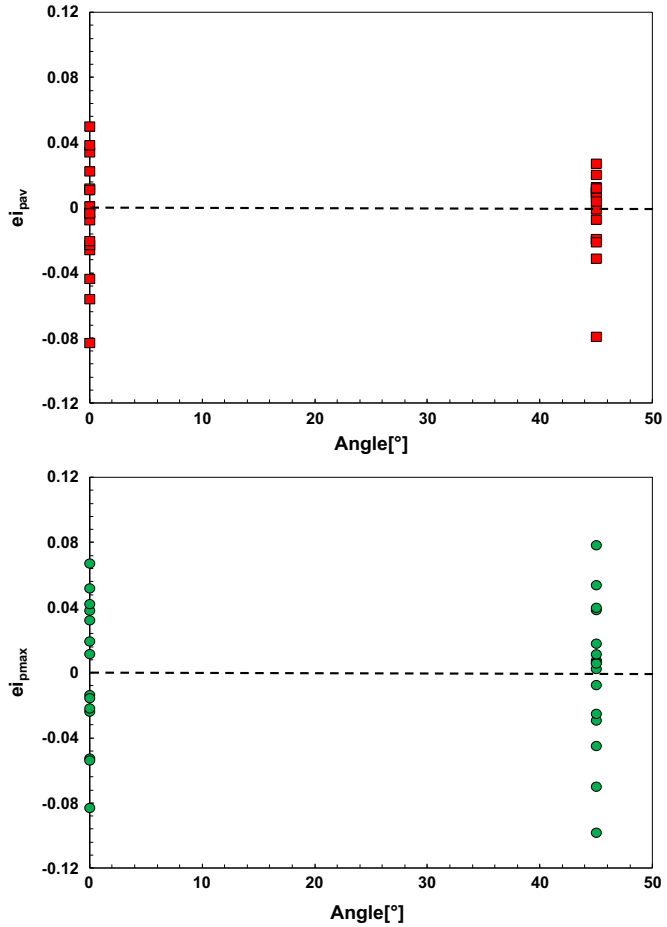

Fig. 38. Residuals of Eq. (12b) (top panel) and Eq. (21) (low panel), vs. the wave angle.

front face of the device, as well as the rise time of the peak of force (Section 6). All those quantities have been modeled as log-normal random variables, the parameters of which have been estimated by a set of semi-empirical equations. In particular for non impacting waves a simplified form of the wave momentum balance permitted to link the expected value of the mean wave pressure to the linear thrust parameter (Eq. (12b)). When applied to the data of Vicinanza and Frigaard, such relationship proved absolutely reliable (Fig. 35), suggesting it can be trustily employed for engineering applications. In principle, the proposed approach might be generalized to other types of maritime structures, such as crown walls at the top of rubble mound breakwaters or caisson breakwaters with sloping face. Given the high correlation with the experimental data exhibited for SSGs, an ad hoc investigation on this point would be indeed desirable.

Also the equation for predicting the maximum wave pressure (Eq. (21)) was found to perform very satisfactorily (Fig. 36); this in spite of the low number of pressure transducers available in the regular wave experiments.

More data is required to check the reliability of the design tools for plunging breakers. In this respect, the most interesting finding of this research seems to be the absence (or the low occurrence probability) of impact events as severe as those observed for vertical breakwaters. This likely owes to two reasons. On the one side, the shallow water depth in front of the device forces the initiation of breaking seawards the *SSG*; from the other side, the relatively mild inclination of the outer plates obliges the breaker to rotate of about 55° prior hitting the wall. Both the previous circumstances favor the trapping of air pockets of significant size beneath the plunging jet, which tend to cushion the impacts.

In the next paper, the authors will tackle the problem of the uplifts acting at the base of the device. At this stage of knowledge, the latter can be modeled as a triangular distribution of pressures with a maximum value equal to the mean peak $\hat{p}_{av}$. Yet, preliminary indications (Vicinanza et al., 2011; Buccino et al., 2011) seem to suggest such approach to be conservative; actually, a lack of phase relative to the peak of the horizontal force should exist, which may lead to both an increase of resistance against sliding and a reduction of the maximum overturning moment. This may significantly reduce the weight necessary to withstand the waves and accordingly the cost of the structure. Along with these major items, the reliability of the formulae proposed in this article will be further assessed by using a larger number of pressure transducers on the front face of the SSG models.

Acknowledgments

The authors gratefully acknowledge Dr. Francesco Ciardulli (ARTELIA Group), Dr.Phys. Andrea Bove (University of Naples "Federico II") and Dr. Pasquale Di Pace (City of Naples) for their assistance in performing the tests.

The work also was partially supported by the EC FP7 Marie Curie Actions People, Contract PIRSES-GA-2011-295162 – ENVICOP project (Environmentally Friendly Coastal Protection in a Changing Climate) and by RITMARE Flagship Project (National Research Programmes funded by the Italian Ministry of University and Research).

References

Allsop, N.W.H., Vicinanza, D., 1996. Wave impact loadings on vertical breakwaters: development of new prediction formulae. In: Proceedings of the 11th International Harbor Congress, Antwerpen, Belgium.

Allsop, N.W.H., Vicinanza, D., Calabrese, M., Centurioni, L., 1996. Breaking wave impact loads on vertical faces. In: Proceedings of the 6th International Conference ISOPE, Los Angeles, published by ISOPE, isbn:1-880653-25-7, Golden, Colorado, USA, vol. 3, pp. 185–191.

Bagnold, R.A., 1939. Interim report on wave pressure research. J. Inst. Civil Eng. 12, 202–206 (Institution of Civil Engineers, London).

Basco, D., 1985. A qualitative description of wave breaking. J. Waterway, Port, Coast. Ocean Eng. vol. 111 (2).

Battjes, J.A., 1974. Surf similarity, Proceedings 14th Coastal Engineering Conference. ASCE, New York, N.Y., pp. 466–480.

Wave Energy Conversion. In: Brooke, J. (Ed.), 2003. Elsevier, Oxford.

Buccino, M., Vicinanza, D., Ciardulli, F., Calabrese, M., Kofoed, J.P., 2011. Wave pressures and loads on a small scale model of the Svåheia SSG pilot project. In: Proceedings of the European Wave and Tide Energy Conference (EWTEC, 2011).

Buccino, M., Banfi, D., Vicinanza, D., Calabrese, M., D.Giudice, G., Carravetta, A., 2012. Non breaking wave forces at the front face of Seawave Slotcone Generators. Energies 5, 4779–4803.
Bullock, G.N., Crawford, A.R., Hewson, P.J., Walkden, M.J.A., Bird, P.A.D., 2001. The influence of air and scale on wave impact pressures. Coast. Eng. 42, 291–312.
Calabrese, M., Buccino, M., 2000. Wave impacts on vertical and composite breakwaters. In: Proceedings of the 10th International Conference ISOPE, Seattle.
Calabrese, M. Allsop, N.W.H. Buccino, M., 2000. Effect of random multidirectional wave fields on wave loads on vertical and composite breakwaters. In: Proceedings of the 27th International Conference on Coastal Engineering, vol. 2. Sydney, Australia, 16–21 July 2000, pp. 1710–1723.
Clement, A., McCullen, P., Falcao, A., Fiorentino, A., Gardner, F., Hammarlund, K., Lemonis, G., Lewis, T., Nielsen, K., Petroncini, S., Pontes, M., Schild, P., Sjostrom, B.O., Sorensen, H., Thorpe, T., 2002. Wave energy in Europe: current status and perspectives 6, 405–431.
Cross, R.H., Sollitt, C.K., 1972. Wave transmission by overtopping. J. Waterw., Harb. Coast. Eng. Div. Proc. Am. Soc. Civil Eng., 295–308.
Cuomo, G., Allsop, W., Takahashi, S., 2010. Scaling wave impact pressures on vertical walls. Coast. Eng. 57, 604–609.
Daniel, P., 1952. On the limiting clapotis. Gravity Waves: Circular No. 521. National Bureau of Standards. pp. 35–38.
Falcão, A.F.D.O., 2010. Wave energy utilization: a review of the technologies. Renew. Sustain. Energy Rev. 14, 899–918.
Ocean Wave Energy. In: Falnes, J. (Ed.), 2002. Cambridge University Press, Cambridge, UK.
Fuhrboter, A., 1985. Model and prototype tests for wave impact and run-up on an uniform slope 1:4. In: Proceedings of the Water Wave Research, Hannover, Germany.
Galvin, C.J., 1968. Breaker type classification on three laboratory beaches. J. Geophys. Res. vol. 73 (12), 3651–3659.
Galvin, C.J., 1969. Breaker travel and choice of design wave height. J. Waterw. Harb. Div. vol. 95 (2), 175–200.
Goda, Y., 1986. Random sea waves and Engineering applications. University of Tokyo Press.
Goda, Y., 1995. Japan's design practice in assessing wave forces on vertical breakwaters, Wave forces on inclined and vertical wall structures. ASCE p. 402.
Hattori, M., Arami, A., 1992. Impact breaking wave pressures on vertical walls. In: Proceedings 23rd Conference on Coastal Engineering. ASCE, pp. 1785–1799.
Hughes, S.A., 2004. Wave momentum flux parameter: a descriptor for nearshore waves. Coast. Eng. 51 (11–12), 1067–1084.
Iribarren, C.R., Nogales, C., 1949. Protection des Ports. XVIIth PIANC Int. Nav. Congress, Lisbon. Section II, Comm. 4, p. 31–80.
Iversen, H.W., 1952. Laboratory study of breakers. Gravity Waves, Natl. Bur. Std. Circ. 521, 9.
Johnson, R.A., Wichern, D.W., 1998. Applied Multivariate Statistical Analysis. Pearson Prentice Hall.
Kirkgoz, M.S., 1995. Breaking wave impact on vertical and sloping coastal structures. Ocean Eng. 22, 35–48.
Kofoed, J.P., Bingham, H., Christensen, E.D., Zanuttigh, B., Martinelli, L., Castagnetti, M., Bard, J., Kracht, P., Frigaard, P., Nielsen, K., Sørensen, J.D., 2010. State of the Art Descriptions and Tasks for Structural Design of Wave Energy Devices. Technical Report no. XX.
Longuet-Higgins, M.S., 1975. On the joint distribution of wave periods and amplitudes of sea waves. J. Geophys. Res. 80, 2688–2694.
Margheritini, L., Vicinanza, D., Frigaard, P., 2009. SSG wave energy converter: design, reliability and hydraulic performance of an innovative overtopping device. J. Renew. Energy 34, 1371–1380.
Marzeddu, A., Gironella, X., 2013. Impulsive wave loads on rigid structure, an experimental approach. In: Conley, D.C., Masselink, G., Russell, P.E., O'Hare, T.J. (eds.). Proceedings 12th International Coastal Symposium (Plymouth, England). Journal of Coastal Research, Special Issue no. 65, pp. 332–337, issn:0749-0208.
Nagai, S., 1973. Wave forces on structures. Advance in Hydroscience, 9. Academic Press, New York and London, pp. 254–324.
Nagai, S., Otsubo, T., 1974. Pressures by breaking waves on composite-type breakwaters. Proceedings 14th Conference on Coastal Engineering, 58. ASCE, pp. 920–933.
Oumeraci, H., Klammer, P., Kortenhaus, A., 1994. Impact loading and dynamic response of vertical breakwaters-review of experimental results. In: Proceeding International Workshop Wave Barriers in Deepwaters, pp. 347–361.
Oumeraci, H., Allsop, N.W.H., De Groot, M.B., Crouch, R.S., Vrijling, J.K., 1999. Probabilistic design tools for vertical breakwaters. Balkema, Rotterdam the Netherlands.
Peregrine, D.H., 2003. Water-wave impact on walls. Ann. Rev. Fluid Mech. 35, 23–44.
Polinder, H., Scuotto, M., 2005. Wave energy converters and their impact on power systems. In: Proceedings of the International Conference of future power systems.
REN21, 2013. Renewables Global Status Report. Institute for Sustainable Energy Policies (ISEP). p. 14.
Svendsen, I.B.A., 2006. Introduction to Nearshore Hydrodynamics. World Scientific.
Takahashi, S., Tanimoto, K., Miyanaga, S., 1985. Uplift wave forces due to the compression of enclosed air layer and their similitude low. Coast. Eng. 28, 191–206.
Takahashi, S., Hosoyamada, S., Yamamoto, S., 1994. Hydrodynamic characteristics of sloping top caissons. Proceedings of International Conference on Hydro-Technical Engineering for Port and Harbor Construction, 1. Port and Harbour Research Institute, Japan, pp. 733–746.
Tanimoto, K., Kimura, K., 1985. A hydraulic experiment study on trapezoidal caisson breakwaters. Port and Harbour Research Institute, Yokosuka, Japan (Technical Note No. 528).
Vicinanza, D., 1997. (In Italian). Ph.D. thesis). Pressioni e forze di impatto di onde frangenti su dighe a paramento verticale e composite.
Vicinanza, D., Frigaard, P., 2009. Wave pressure acting on a seawave slot-cone generator. Coast. Eng. 55, 553–568.
Vicinanza, D., Ciardulli, F., Buccino, M., Calabrese, M., Kofoed, J.P., 2011. Wave loadings acting on an innovative breakwater for energy production. J. Coast. Res. 64, 608–612.
Vicinanza, D., Margheritini, L., Kofoed, J.P., Buccino, M., 2012. The SSG wave energy converter: performance, status and recent developments. Energies 5 (2), 193–226.
Vicinanza, D., Contestabile, P., Harck Nørgaard, J.Q., Lykke Andersen, T., 2014. Innovative rubble mound breakwaters for overtopping wave energy conversion. Coast. Eng. 88, 154–170.
Zanuttigh, B., Van der Meer, J.W., 2008. Wave reflection from coastal structures in design conditions. Coast. Eng. 55 (10), 771–779.
Zelt, J.A., Skjelbreia, J.E., 1992. Estimating incident and reflected wave field using an arbitrary number of wave gauges. In: Proceedings of International Conference on Coastal Engineering. vol. I, 777–789.